Department of Mechanical and Aerospace Engineering

CFD Modelling and Analysis of the Temporal Impact of Leading-Edge Erosion on the Aerodynamic and Operational Performance of Wind Turbine Blades

Author: Sonny Cain

Supervisor: Dr. Nick Kelly

A thesis submitted in partial fulfilment for the requirement of degree in

Master of Science in Sustainable Engineering: Renewable Energy Systems and the Enivironment

2023

Copyright Declaration

Abstract

As the world shifts toward a sustainably powered future, wind energy has emerged as a leading solution for producing electricity at scale. These technologies have seen accelerated deployment throughout the world in both offshore and onshore regions. However, due to the dynamic environment in which they operate, wind turbines are exposed to continued impact with different airborne particles such as rain, hail and sand. These continued impacts cause the blade surfaces to erode through a phenomenon called Leading Edge Erosion which has significant impacts on the aerodynamic and operational performance of these technologies which grows greater with time.

This paper aims to model Leading Edge Erosion using the NACA 4412 aerofoil within CFD software and a negative surface roughness boundary condition and analyse the impact of this erosion on the aerodynamic performance. Specifically, the Lift and Drag Coefficients produced by the blades. The paper also aims to investigate the implications of these impacted lift and drag coefficients on the operational performance of wind turbines, such as their annual energy production. Furthermore, this paper aims to develop a framework for estimating the time for the different stages of erosion begin.

The results showed that Leading edge erosion has significant impacts on the aerodynamic performance of the wind turbine, with reductions in the lift coefficient ranging from 2.48% to 35.6% and increases in the drag coefficient ranging from 22.94% to 153.15%. These aerodynamic impacts translated to an estimated annual energy production loss ranging from 1.65% to 18.4%. The results of the erosion framework estimated that the coating materials used on wind turbine blades, could fail after 6-19 years dependent on the rainfall rate of the region.

The implications of these findings are significant to the financial viability of the UK wind energy sector, with yearly average losses of over £161 million. The NPV of wind farm projects was also negatively affected, showing an £140 million reduction in the NPV of the recently developed Hornsea 2.

Acknowledgements

Firstly, I would like to thank Dr. Nick Kelly for his supervision and support throughout the duration of this project.

I would also like to thank my family and friends for providing unwavering support throughout the entirety of this project. I would also like to say thank you to family friends Sue and Phil Stockton for their proofreading.

Table of Contents

List of Figures

List of Tables

Abbreviations

AEP	-	Annual Energy Production
AoA	-	Angle of Attack (°)
BPA	-	Bisphenol-A
C_d	-	Coefficient of Drag
C_l	-	Coefficient of Lift
C_p	-	Coefficient of Power
LEE	-	Leading Edge Erosion
TSR	-	Tip Speed Ratio

1.0 Introduction

As the world transitions toward a sustainably powered future, renewable energy technologies are seeing accelerated adoption globally. Among these, wind energy production has emerged as a leading contender, harnessing the power of the wind to generate electricity on a large scale. This technology has seen particularly wide scale deployment in the UK as a means of producing clean electricity for a range of applications. In 2022, British wind farms reported a record contribution to national electricity, at 26.8% [10], with offshore wind being responsible for 14.1% respectively and thus, highlighting the significance of these technologies to the existing and future energy networks.

As of 2023, the UK has over 28GW of installed capacity, 14GW onshore and 14GW offshore [11] which are responsible for the production of the UK's electricity demand. In a global context, global cumulative capacity grew by 77.6GW to 906GW in 2022 [3], with accelerated installation in offshore wind in particular.

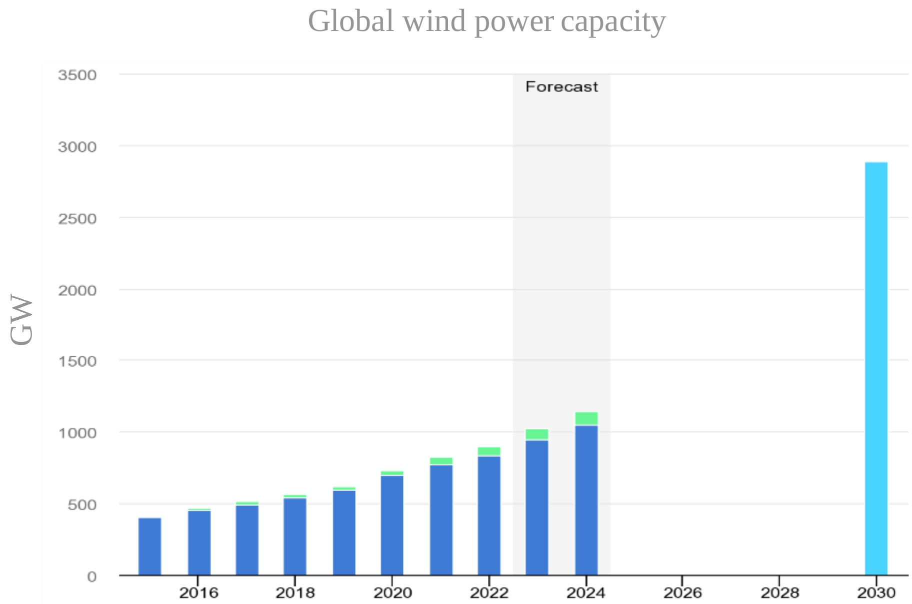

Figure 1 - Global Wind Capacity [3]

To meet the ambitious net-zero targets outlined by the UK government as part of the Paris agreement, the UK projects that offshore wind capacity will continue to increase to around 50GW by 2050 [12] while projecting an onshore capacity of 30GW [13] by 2030. With these ambitious targets in place, wind turbine manufacturers are constantly developing larger diameter turbines, operating at higher tip speeds to produce this energy more economically. Figure 2 illustrates the increase in both wind turbine diameter since the inception of the of the technology.

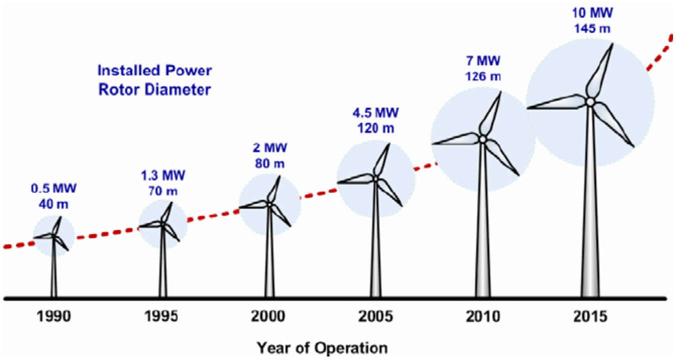

Figure 2 - Increase in Turbine Diameter with time [6]

However, one issue which has become prevalent, due to increasing turbine diameters and tip speeds along with the dynamic environment in which these technologies operate within, is Leading Edge Erosion (LEE). LEE is the phenomena in which material is removed from the surface of the turbine blades, specifically the leading-edge, due to continued high impact collisions with airborne particles such as rain, hail, ice, and sand. The issue has become more prominent in recent years due to the increase in turbine size and the consequent higher operating tip-speeds. An example of this erosion for different periods of service is shown in Figure 3.

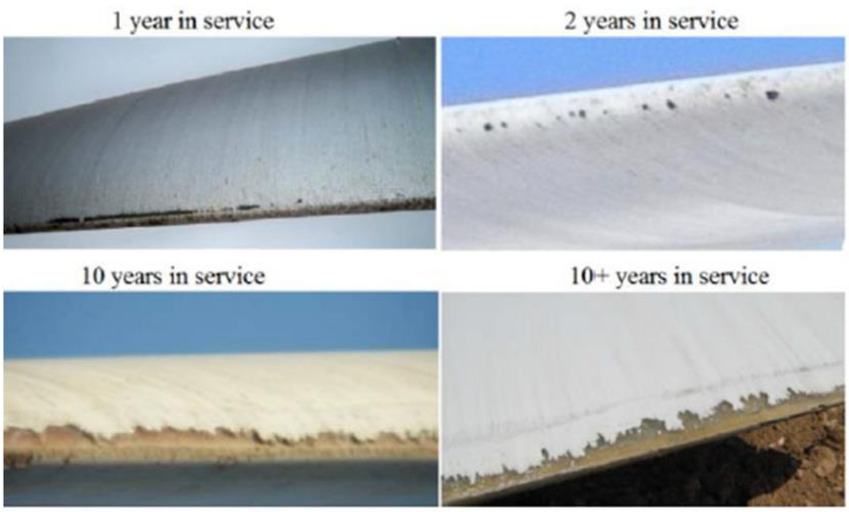

Figure 3 - Observed erosion for different periods of operation [14]

The removal of material causes a roughening of the leading edge which can have significant impacts on the aerodynamic properties of the blade profiles. These aerodynamic changes have significant effects on the efficiencies and power generation of turbines in operation and these effects grow greater with time. The severity of these losses has been estimated to range from between 1-70% [15-17] dependent on the level of erosion that is present. Therefore, wind turbine operators and developers can see significant financial implications due to lost revenue paired with logistical implications through the monitoring, maintenance, and repair of these damages throughout the 25-year operating lifespan of these technologies. Furthermore, these damages pose environmental challenges due to the complex composite materials which are being eroded and emitted to the surrounding environment. This presents a significant challenge for industry to understand how these different erosion stages develop temporally in order to develop suitable coating materials to delay their development.

Therefore, the phenomena of LEE on wind turbine blades is one of increasing importance to both industry and research who aim to accurately model this impacts and develop systems to combat these effects. Within this paper, the temporal impacts of LEE on the aerodynamic and operational performance of wind turbines are modelled and analysed with the aim of developing the current understanding of this phenomenon. Within the field of research, there have been many approaches to modelling leading edge erosion, from numerical models to experimental setups. One approach which hasn't been explored in detail is the use of CFD software to model the aerofoil and modelling the erosion as a negative surface roughness.

This paper will explore the effects of leading-edge surface roughness on the aerodynamic and operational performance along with the temporal progression of the surface roughness. Furthermore, the aims of this paper are to develop a CFD model which can emulate the behaviour of an aerofoil with a varying surface roughness to represent leading-edge erosion. The study also aims to develop a framework which can analyse the temporal progression between the different erosion stages for different regions. These specific project aims, and the related objectives are further discussed in Section 3.0.

2.0 Literature Review

In this section the published literature within the field of research is reviewed to establish an understanding of the previous work regarding the previous approaches to modelling LEE. Section 2.1 provides a brief review of the underlying principles of aerofoil theory and how these are affected by LEE. Section 2.2 explores the behaviour, characteristics, and categorisation of leading-edge erosion and the variation in impact between particles. Section 2.3 critically reviews the previous approaches to modelling leading edge erosion. Section 2.4 reviews the current understanding between the impact of LEE and the annual energy production capability of wind turbines, followed by a final section identifying the key research gaps used to create the project aims and objectives.

2.1 Aerofoil Theory

The aerofoil is a cross-sectional shape, designed with a curved surface, to provide an optimal ratio between lift and drag for the desired application. In the case of wind turbine blades, the lift-to-drag is optimised to increase the rotation of the rotor and produce energy. The component of lift is generated perpendicular to the direction of motion and the component of drag is produced parallel to the direction of motion. An example of an aerofoil and the directions of these forces can be seen in Figure 4.

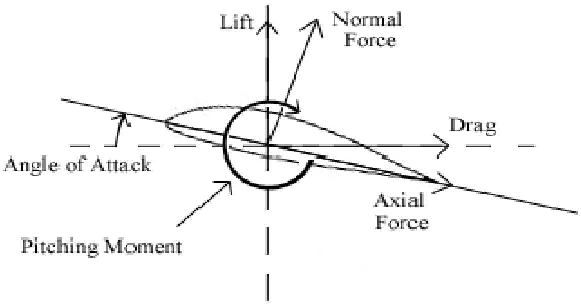

Figure 4 - Aerofoil force generation [18]

An aerofoil can be divided into four main sections: the leading edge, the trailing edge, the upper surface, and the lower surface. Between these sections there are several key measurements, such as the Angle of attack (AoA) and chord length, which are varied between application. Figure 5 illustrates these different sections and measurements.

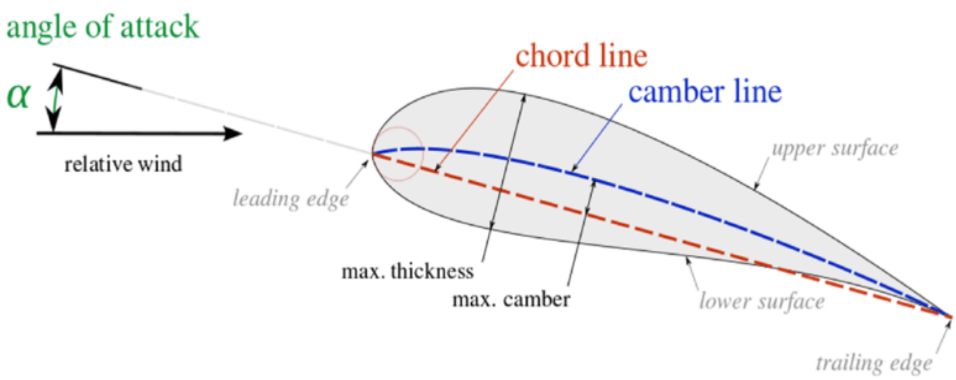

Figure 5 - Aerofoil key measurements [7]

The oncoming airflow is split by the leading edge which diverts the flow to the lower side and upper side in way that creates a favourable ratio of lift and drag, this subjects the lower side to a higher pressure, often referred to as the pressure side, and the upper side to lower pressure, called the suction side. In the case of a wind turbine, the wind flow across the blade and the pressure difference between both sides causes the blades to spin around the fixed rotor.

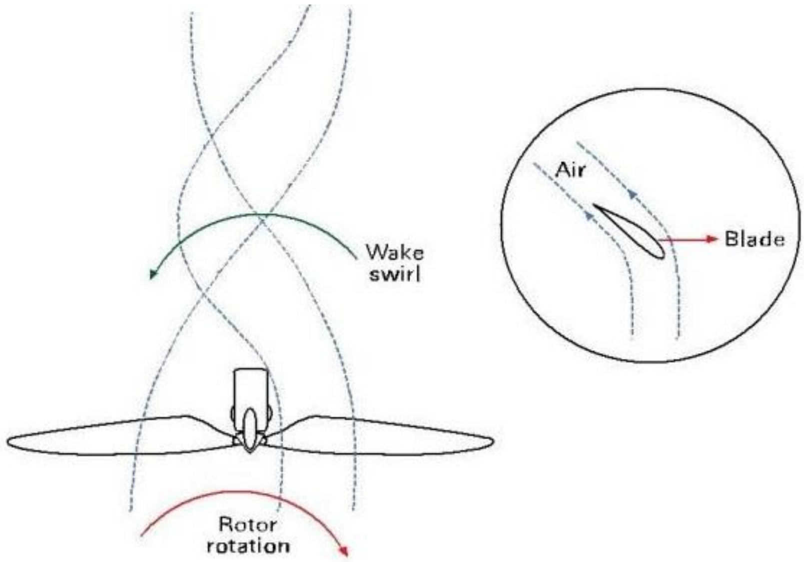

Figure 6 - Airflow over a turbine rotor [8]

In the application of a wind turbine blade, aerofoils are designed to produce a high lift to drag ratio to increase rotational speeds and the energy production potential of the turbine. In order to increase the generated lift-to-drag ratio, turbines will install pitch control in order to alter the AoA during operation to ensure the lift-to-drag ratio is optimised during periods of operation [6, 19]

2.1.1 Lift Coefficient

The lift produced by the blades is the force which drives the rotation of the turbine, and it is heavily dependent on a factor called the Lift Coefficient which can be calculated using:

$$C_L = \frac{2F_L}{\rho \cdot V^2 \cdot A}$$

Where;

F_L = Lift Force (N)

ρ = Density (kg/m3)

V = Velocity (m/s)

A = Area (m2)

The lift coefficient is influenced by various factors, including the shape and design of the wind turbine blade, the AoA and the flow conditions. The coefficient of lift is also heavily dependent on the surface of the aerofoil, with rougher surfaces producing less lift than smoother surfaces. The impact of surface roughness in the case of a wind turbine blade will be further discussed in Section 2.1.3.

2.1.2 Drag Coefficient

When flow passes over a blade, it generates lift due to the pressure difference between the upper and lower surfaces of the blade. However, the creation of lift also leads to the generation of induced drag. A schematic showing the generation of induced drag is shown in Figure 7.

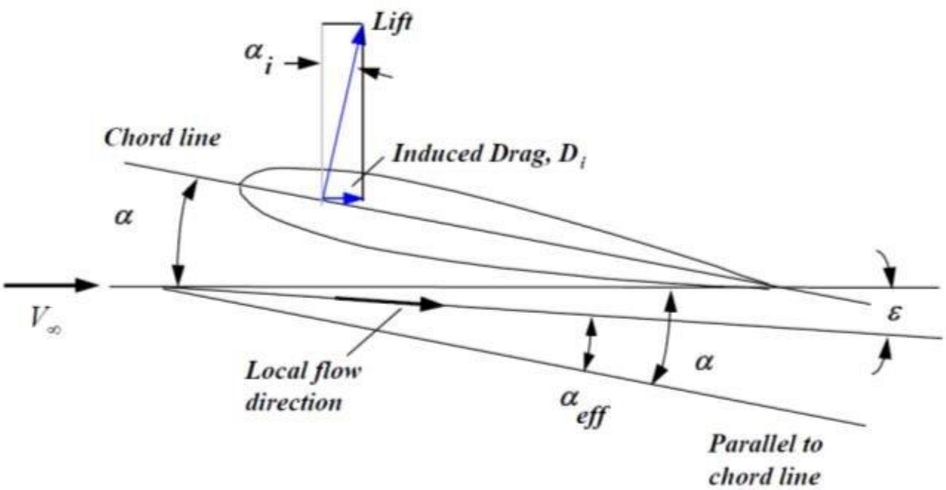

Figure 7 - Induced Drag over an aerofoil [20]

Another type of drag that is produced is profile, or form drag, which occurs through the frictional resistance of blades as they pass through the air [21]. Profile drag does not change significantly with angle of attack but increases with the speed of oncoming airflow [22]. A schematic showing the relationship between the different types of drag and airflow speed is shown in Figure 8.

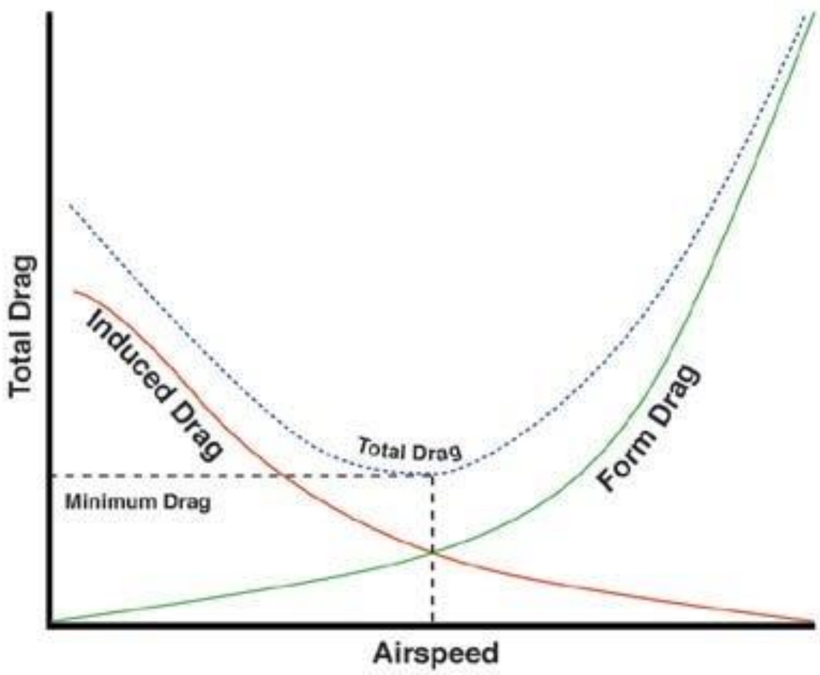

Figure 8 - Form, Induced and Total Drag vs Airspeed [22]

Both profile drag and induced drag are contained within the Drag Coefficient [23] which is a number that represents the resistance of an object relative to its frontal area as it moves through a fluid [24]. The Drag Coefficient is described using the following equation:

$$C_D = \frac{2F_D}{\rho \cdot A \cdot V^2}$$

F_D = Drag Force (N)

ρ = Density (kg/m3)

V = Velocity (m/s)

A = Area (m2)

Both the lift and drag coefficients are influenced by the roughness of the surface of the object that is passing through a fluid. Therefore, the next section begins to explore how LEE impacts both the lift and drag that is produced by an aerofoil in the application of a wind turbine blade.

2.1.3 Influence of LEE on Lift and Drag

LEE creates a roughened leading-edge which disrupts the flow of wind over the blades [2, 9, 25-27]. This roughened leading-edge and consequent disrupted flow can have significant effects on the lift and drag coefficients produced by the blades [9, 16, 27]. This impact on lift and drag is caused by the roughness at the leading-edge which causes an earlier transition from laminar to turbulent flow, causing premature separation of the flow from the surface [16, 28]. A visual representation of this premature separation is shown in Figure 9.

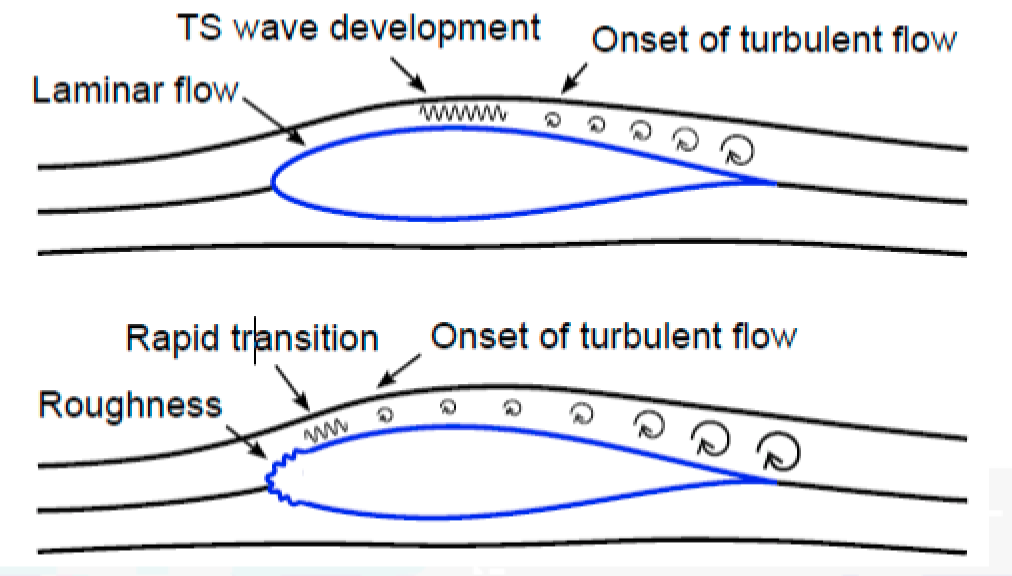

Figure 9 - Flow behaviour for smooth and rough leading-edge [28]

This earlier separation reduces the lift that is generated by the aerofoil whilst concurrently increasing the drag that is produced [16, 27, 29, 30]. In the case of HAWTs, the production of lift is directly related to the energy production, therefore, minimising the drag whilst maximising the lift is key to extracting the optimal energy from the wind resource, highlighting the need to prevent or delay the onset of the roughened leading edge. The next section will briefly review the types of aerofoils used within the industry today, with their advantages and limitations along with the selection of an aerofoil for this analysis.

2.1.4 Aerofoil types used in Wind Turbines

The blade aerofoil selection is an important design decision during the manufacture of a wind turbine. This selection process is complex due to the number of different properties between the different aerofoil families [31]. Within this section, three aerofoil families which have been widely used for wind turbine blades will be discussed, with information on their designs and key characteristics.

2.1.4.1 NACA Aerofoils

The NACA family of aerofoils have many applications in aerodynamics, but their most common use is within aircraft wings and wind turbine blades. These aerofoils are categorised by the complexity of their shapes and named using a four, five or six-digit number sequence.

There has been significant research into the applications of the different aerofoils, with many four-, five- and six-digit series aerofoils featuring in wind turbines today. Considering the simplicity of the shape for the ease of modelling and the optimal performance characteristics [32], the NACA 4412 will be selected for the analysis within this study. This aerofoil has demonstrated to have the highest rotation rate whilst also demonstrating higher performance than its NREL competitors in smaller scale wind turbines [33, 34]. However, this aerofoil in practice may not be suitable for an entire blade profile in a larger scale turbine and may only make up a smaller section of a more complex blade. Moreover, these blades are susceptible to the impacts of LEE [5] and this may exacerbate the effect on the aerodynamic and operational performance. Despite this, the NACA 4412 has demonstrated that it is capable of being the sole aerofoil for low wind speed, low Reynold number wind turbine applications [35].

2.1.4.2 NREL Aerofoils

The NREL has developed several aerofoil families since 1984 [5].. Like other aerofoil families, they are also categorised on the thickness of the aerofoil as a measure of the total chord length [5] with two categories of "thick" and "thin" aerofoils which have a thickness of 0.16c-0.21c and 0.11c-0.15c respectively. Table 1 shows some of the varying aerofoils used for different rotor diameters.

Table 1 - NREL Aerofoils [5]

Blade Length (meters)	**Generator Size (kW)**	**Thickness Category**	**Airfoil Family (root———————tip)**			
1-5	2-20	thick		S823		S822
5-10	20-150	thin		S804	S801	S803
5-10	20-150	thin	S808	S807	S805A	S806A
5-10	20-150	thick		S821	S819	S820
10-15	150-400	thick	S815	S814	S809	S810
10-15	150-400	thick	S815	S814	S812	S813
15-25	400-1000	thick		S818	S816	S817

For use within the blades of a wind turbine, the NREL is a commonly used family. NREL aerofoils benefit from better lift to drag ratios than competitors and a lower sensitivity to surface roughness [5]. The effectiveness of the NREL family of aerofoils is supported in a study by Mouhsine [36] who also highlight their capabilities to meet the requirements for wind turbines [36]. However, wind turbine blades that are made up of a NREL aerofoil, feature many different shapes at different positions along the length of the blade, which would require considerable 2D analysis or a 3D model which requires significant computation [37].

2.1.4.3 Delft Aerofoils

Delft University developed a series of aerofoil dedicated to wind turbine applications. Which have a significantly higher thickness for applications in large diameter turbines. These aerofoils benefit from higher lift-to-drag ratios and higher stability due to their increased thickness. These profiles are also less susceptible to impacts from surface roughness [38, 39]. However, due to the lesser amount of available literature for model validation, this aerofoil family was not selected for analysis within this paper.

2.1.4.1 Selection of Aerofoils

The criteria for the selection of an aerofoil will heavily rely on the lift to drag ratios for the different aerofoil types. The NACA aerofoils have demonstrated to have better lift-to-drag performance than their NREL counterparts [32]. This comes at the expense of some blade stability; however, this analysis will only consider the impact on lift and drag which suggests that the NACA aerofoil family is more suitable for this analysis. The properties of the NACA aerofoils have been widely researched for an array of different applications [34, 40, 41] including wind turbines [32, 33, 35, 42] which will allow for validation of the results of this paper. Due to this, a NACA aerofoil will be selected over the Delft aerofoil due to the greater availability of literature on the aerodynamic performance of these aerofoils and their applications.

One specific NACA aerofoil which has been widely analysed for wind turbine applications is the NACA 4412 [33, 35, 42-44]. However, this aerofoil has often been analysed at low Reynolds numbers for wind turbine applications [42, 45], which allows for this paper to address a gap within the literature through measuring the impact of LEE on both aerodynamic and operational performance of this aerofoil at higher Reynolds numbers. The next section will investigate the characteristics of LEE on aerofoils used in wind turbine applications along with the categorisation of the different erosion stages and the impact of airborne particles on LEE.

2.2 Leading Edge Erosion

As previously mentioned, LEE is the phenomenon in which material is damaged or removed from the surface of the blade of a wind turbine, increasing surface roughness and reducing aerodynamic performance [46].

The leading edge is the most common area for erosion as it experiences the greatest friction with the wind and other air or windborne particles as the blade rotates. Over the operating lifespan of a wind turbine, the level of LEE can vary from minor erosion (small pits and gouges) [47] to severe erosion where the blade composite has become delaminated exposing the blades composition [48].

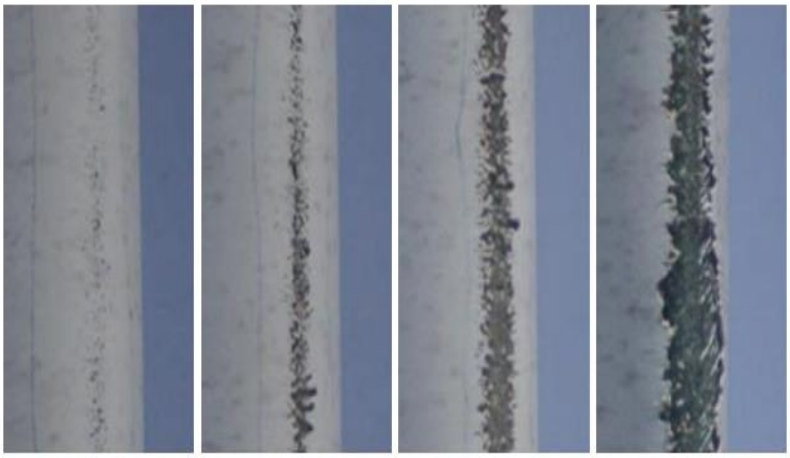

(a) Level 1 (b) Level 2 (c) Level 3 (d) Level 4

Figure 10 - Levels of leading-edge erosion [1, 2]

The areas of removed material will disturb the flow causing premature separation, resulting in increased drag and reduced lift and consequently lower energy production [17]. There are many factors that dictate the rate and severity of leading-edge erosion, such as rotational velocity and the blade composition, but the collision with airborne particles is the driving factor in determining the rate and severity of leading-edge erosion [49]. Therefore, the rate at which LEE develops is strongly related to the meteorological characteristics, such as frequency and intensity of rainfall, of the local region [2, 50-52]. The presence of multiple airborne particles, such as sea aerosols and rain droplets in the case of an offshore wind turbine or sand and insect build up for an onshore wind turbine, have been found to significantly accelerate the rate in which erosion develops [53].

This section will review the prior research into the characteristics of the different stages and the different variables which will influence the rate at which these LEE stages develop. Section 2.2.1 will review the specific characteristics at each stage and the current understanding of how these stages develop temporally. Section 2.2.1 will review the existing literature on the attempts to understand erosion development and Section 2.3 will review the understanding of the impacts on LEE from different airborne particles, specifically rain and hail.

2.2.1 LEE Characteristics

Erosion is characterised by the number of pits and gouges and the level of delamination on the surface of the blade [9, 54, 55]. The categorisation criteria for the different Erosion Severity Stages (ESS) is shown in Table 2.

Table 2 - Erosion categorisation [9]

Table I. Specifications of the nominal erosion features.

Feature	Depth/Diameter	Leading edge coverage
Pits (*P*)	0.51 mm (0.02 in)	0–50.8 mm (0–2 in)
Gouges (*G*)	2.54 mm (0.10 in)	0–50.8 mm (0–2 in)
Delamination (*DL*)	3.81 mm (0.15 in)	0–4.57/9.14/18.29 mm (0–0.18/0.36/0.72 in)

Table II. Test matrix with the approximate number of pits (*P*), number of gouges (*G*), and magnitude of leading edge delamination (*DL*) on the upper surface of the erosion model for each case tested.

	Type A	Type B	Type C
Stage 1	100*P*	—	—
Stage 2	200*P*	200*P*/100*G*	—
Stage 3	400*P*	400*P*/200*G*	400*P*/200*G*/*DL*
Stage 4	—	800*P*/400*G*	800*P*/400*G*/*DL*+
Stage 5	—	—	1600*P*/800*G*/*DL*++

The different stages of erosion are a topic which has been widely researched by industry and the scientific community [9, 26, 56, 57]. Within the literature, it is largely agreed that coating materials of wind turbine blades experience an initial stage of no mass removal, called the incubation period. This is followed by a state of accelerated steady state mass removal which then plateaus beyond the most severe stages of erosion. The current industry standard usually only considers stages 1, 3 and 5 as these indicate a clean surface, the end of the incubation period and the failure of the coating material respectively [56].

2.2.2 LEE development

There have been different approaches into relating the stage of erosion to the stage of mass removal. One approach which is widely cited within the field of research is a study by Nash who aimed to develop a staged approach to the erosion of coating materials [56]. Nash used an experimental setup to measure the time taken for the erosion to develop upon a material surface, then estimating the energy that is transferred from the particles to the material surface. This allowed for the energy required to reach each erosion stage to be estimated. Nash found that the energy to reach the end of the incubation period was 4400J, whilst the energy required to reach stage 5 erosion was 5600J. This agrees with the literature, as the number of impacts require to surpass the incubation period is significantly greater than the number of impacts to reach stage 5 erosion, suggesting that the erosion from stages 1 to 5 is not linear, but is accelerated beyond the incubation period.

However, much of the work based on Springer's model [58, 59] and the Palmgren-Miner Rule [60], suggests that the end of the incubation period is once the failure of the material has occurred. These approaches use the material properties of the coating materials to estimate the number of impacts required to cause failure within the coating material. Once this failure has occurred, the incubation period has ended, and the material is said to be entering the more severe erosion stages. Law utilised this approach using operational wind farm data to validate their methodology [53]. The wind farm data provided a length of time in operation and the level of observed erosion, allowing for comparison between the field data and the results of the numerical approach. However, the results of the numerical approaches did not accurately reflect the operational data, suggesting that the use of the sole use Miner rule within a model of this type was not suitable due to the linearity of the miner rule [53, 61].

Another study which used this more successfully, by D. Eisenberg [2], used the principles of the Miner rule to estimate a damage rate. Eisenberg also used cloud geometry, rain intensity relationships and impingement efficiencies to estimate the number of impacts on the material surface per unit m2 of surface. The model proved to be successful and provided a proportional relationship between damage rate per second and two meteorological variables: the Rainfall Intensity and the Impact Velocity [2]. The model and its relationships were validated with operational data and by Siemens Gamesa and the authors aim to develop these relationships into industry standard for prediction of erosion due to rain droplet impact [2]. However, Eisenberg's study does disagree with the staged approach by Nash as the assumption is made within the paper that beyond the incubation period, erosion rate is linear, whereas Nash and other studies within the literature suggest that there is a period of accelerated erosion beyond the incubation period.

Between these different approaches, the length of time for the onset of erosion varies. The length of time also varies with data observed from operational wind farms. This suggests that there is a literature gap for a model which can comprehensively predict the stage of erosion for a number of rain droplet impacts whilst also accurately a timeframe for the development of erosion. Within this paper, principles from both Springer and Nash will be used to predict the number of impacts for the failure of the coating material and the length of the incubation period.

The next section will investigate the previous literature regarding the impact of different airborne particles.

2.3 Rain Droplet Erosion

Rain is the airborne particle that is most responsible for contributing to leading edge erosion, especially in offshore wind farms [50, 62]. The erosive effects of rain droplets have been analysed in many studies [51, 53, 62, 63] with varying approaches from dynamic modelling to numerical and experimental models. The results of these studies have led to the development of predictive fatigue-based models for estimating the erosive damage caused by rain droplet impingement on a surface [64].

2.3.1 Frequency of rainfall

The fatigue-based models are based on formulas which are dependent on the number of droplets. Therefore, the erosive effect of the impact of rain droplets on the surface of a turbine blade is highly dependent on the frequency and intensity of rain in the local region. In 2022, the UK saw an average of 1,090 millimetres of rainfall, with an average of 179 rain days [4]. A map of the rainfall within individual regions can be seen in Figure 11.

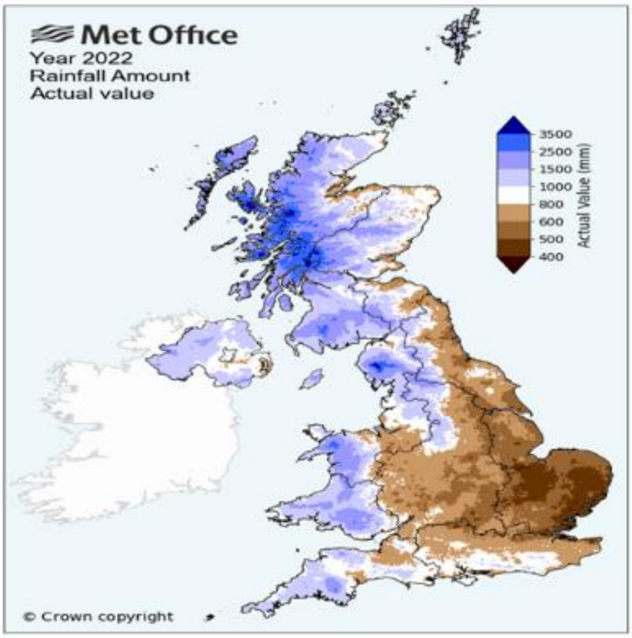

Figure 11 - Rainfall Map 2022 [4]

Figure 5 highlights that western and central regions within the UK suffer from greater rainfall than others [4], suggesting that turbines in these regions would be subject to greater rain erosion than other areas. This is also supported in a study by Stack [52] which developed turbine rain erosion maps based on geological data, which also highlights these areas as being prone to significant leading-edge erosion, shown in Figure 12.

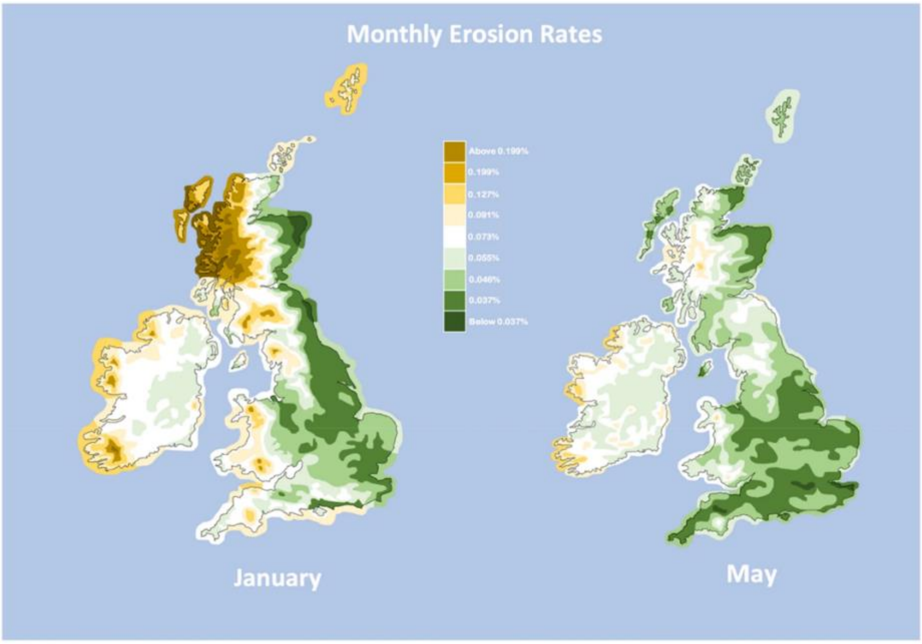

Figure 12 - UK Erosion Map [52]

2.3.2 Rain Droplet Impacts

The literature on rain droplet impacts agrees there is the existence of an 'incubation period' in which there is no removal of material due to rain droplet impacts and this considered in literature and industry to be the operating lifespan of turbine blade coating systems. Beyond this period, it is generally agreed that there is then a linear, accelerated rate of surface mass loss. The relationship between impacts per area and mass loss can be seen in Figure 13.

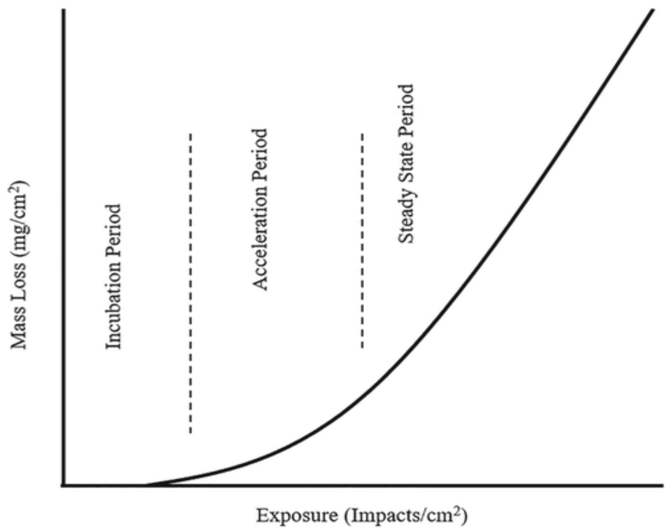

Figure 13 - Mass Loss vs Impact per cm^2 [53]

The literature generally agrees the two main forces to be considered in a rain droplet erosion model are the Water Hammer Pressure and the resulting stress cycle from the resulting

Rayleigh wave [58, 59, 64]. However, there is some disagreement between the indications of each stage, which will be further discussed in Section 2.5 which discusses the previous attempts to adapt these relationships into models for predicting coating material lifetimes.

2.4 Hailstone Erosion

Hail is another airborne particle which has an effect on the LEE of wind turbine blades [51, 53, 65]. The effect of hail on leading edge erosion is dependent on the frequency of Hail within the region, the size and concentration of hailstones in hailstorms and the type of impact with the blade surface. The available literature on these parameters will be reviewed in this section.

2.4.1 Frequency of hail

Hail is another airborne particle which has a significant effect on the LEE of wind turbine blades. Hail is solid precipitation in the form of small balls or pieces of ice often referred to as 'Hailstones'. These hailstones are formed in storm clouds as raindrops pass up to the top of clouds, where the temperature is much lower and these raindrops freeze [4].

The impact of hail on LEE is dependent on the frequency of hail within the region. In the UK, Hail is most common during spring and summer due to the heat energy in the sea, with regions in the west and north of the UK being most affected [4] and this can be seen in Figure 7.

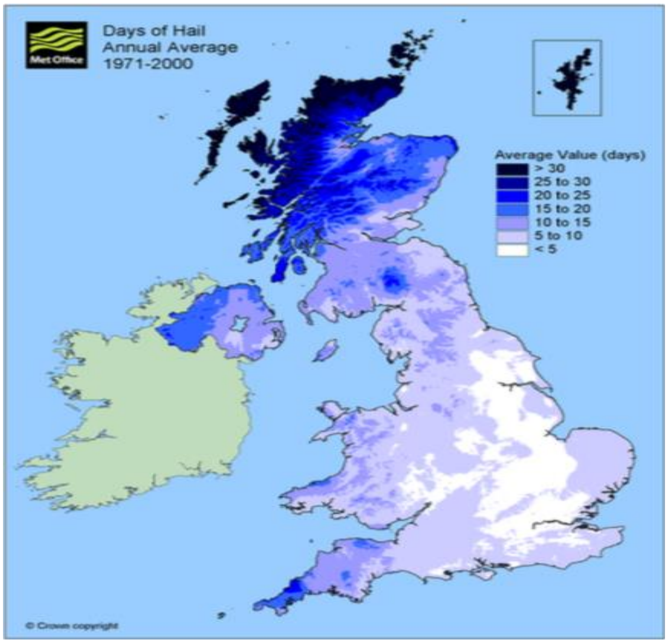

Figure 14 - Hail intensity map [4]

Therefore, it can be said that the impact of hail in Southern and Eastern regions can be considered minimal, but the effect of Hail will still have to be considered for wind farms across

England. This agrees with the available information on the regional intensity of rainfall as the areas affected by rainfall are also affected by hail [4].

However, the occurrence of hailstorms is rare, with hail occurring on less than 10 days within an annual period. The occurrence of hailstorms in Scotland is considerably higher, at around 30 days per annual period [4, 66], which suggests that the impact of hailstones on LEE is an imperative consideration for wind farm constructors in these regions.

2.4.2 Hailstone characteristics

It is generally agreed within literature and meteorological data that Hailstones are frozen water droplets with a diameter greater than 5 millimetres [4] with frozen pellets smaller than this being classified as snow or ice pellets. Hailstones are also frozen within the cloud before they descend downward and land as frozen droplets, whereas ice pellets and freezing rain undergo state changes during descent. The material properties of hail, such as the density, hardness and Youngs modulus vary between studies. Of these material properties, density is the property that has the most variance between studies as it changes with the size of hailstone.

Literature suggests a lower end for the density of hail at around 0.45g/cm3 [67], however, more recent studies have found the mean densities of hailstones to range between 0.8-0.9g/cm3 [68]. These wide ranges highlight that the variance in weather conditions for hail will result in ununiformed distribution of the size and material properties of hailstones for a given location. While there is variation between the exact density of hailstones, there is a consensus amongst researchers that the density is lower than that of pure ice, at 0.917g/cm3.

2.5 Modelling of LEE

This section will review the previous approaches to modelling LEE to establish an understanding of the variances in observed results along with the key findings and limitations of the different approaches in order to find the relevant gaps to address within this paper. Section 2.5.1 discusses the computational fluid dynamics (CFD) approaches, in particular the different erosion geometries and model types. Section 2.5.2 explores the existing numerical methods used to predict coating lifetimes along with their fundamental principles. Finally, Section 2.5.3 reviews the experimental methods used as basis and validation for both the numerical and CFD approaches.

2.5.1 CFD Modelling of LEE

To validate the numerical methods used to estimate the severity of leading-edge erosion, CFD models are often used to relate the severity of erosion to a change in aerodynamic performance of the blades. Much of this work is done by using fluid modelling software such as ANSYS to investigate the change in fluid behaviour because of leading-edge erosion [17, 26, 50, 69, 70]. Some studies have also used an eroded aerofoil in wind turbine specific simulation software to estimate the effect on annual energy production [69]. However, there are differences in the ways that the leading-edge erosion is modelled across the literature, with some studies opting for a modelling the physical geometry of an eroded aerofoil [69] and others relating the severity of erosion to a surface roughness [70]. This section will review and comment on the differences between the relevant studies within the literature.

One approach of modelling leading edge erosion that has been used within the literature is to create a 3D model of an aerofoil and include the erosion within the model geometry. A paper which used this approach written by Carraro [69] compared the difference between 2D and 3D models for investigating leading edge erosion. Both the 2D and 3D models had the eroded features in the model geometry, and these can be seen in Figure 15.

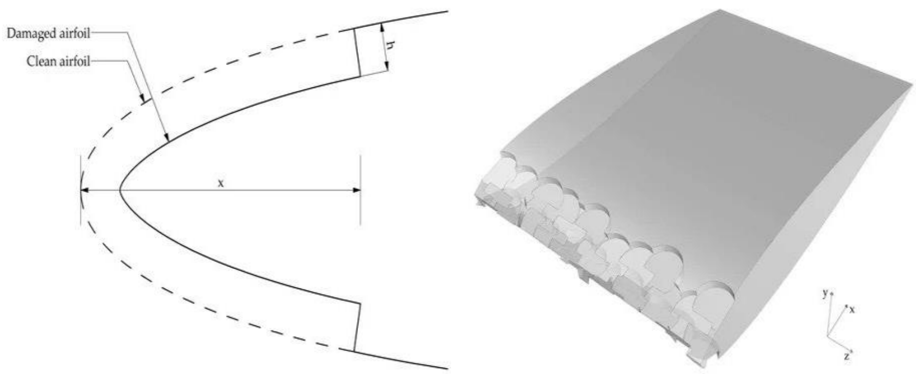

Figure 15 2D (left) and 3D (right) eroded blade geometry [69]

Within the literature, it is generally agreed that 2D aerofoil models can simulate the effects of leading-edge erosion at a much lower computational cost [69]. A highly regarded study into the use of a 2D aerofoil model for investigating leading edge erosion by Ravishankara [70] used a CFD model of a 2D aerofoil with varying surface roughness to account for the different stages of erosion. The defined roughness was based on a study by Sareen [9] who had outlined the number of pits, gouges, and the level of delamination for each stage of erosion, along with the depth, width, and locations of these defects. The study adapted these surface deformities into an equivalent sand grain roughness using a relationship proposed by Flack [71]. From this, the coefficients of lift and drag for different angles of attack and two different erosion stages were calculated.

The results of the investigation also highlighted that a Spalart-Allmaras (SA) model was more suitable than a Shear Stress Transport (SST) model for this type of investigation [70]. This is because the SST model did not match the experimental data for empirical models, whereas the SA model was validated against experimental data for two different aerofoils [70] and required a less fine mesh to achieve an independent solution. Therefore, for the CFD analysis within this study, a 2D SA model will be used with a surface roughness boundary condition to investigate the effects of leading-edge erosion.

However, this study did not investigate how the erosion developed temporally between stages, rather just investigated the aerodynamic impact for the two chosen erosion stages. Furthermore, when using the developed equivalent sand-grain roughness approach, only two stages of erosion were investigated and as these were more severe stages of erosion, the lift, drag and AEP loss results were toward the higher end of the range of values estimated by other studies [9, 15, 16, 53]. This highlights a gap within the literature to produce a framework which can investigate a wider range of erosion stages using surface roughness along with a temporal analysis of the erosion development.

2.5.2 Numerical Modelling of LEE

There have been many different approaches to modelling the leading-edge erosion of a wind turbine blade. Two commonly used methods within the literature are purely numerical approaches or CFD modelled approaches, or a mix to serve as validation for each other. This section will describe the previous work on the development of numerical models for predicting and analysing leading edge erosion.

Many of the previous numerical model studies, are based on the work of Springer [58, 59, 61], who in his Erosion by liquid impact paper, developed a model which predicted the level of surface mass removal for a surface which faces continual impact from rain droplets. Within this paper, Springer proposes the existence of a ‘incubation period’ in which no material is removed from the surface, and very little erosive effect. Beyond this period, there is a period of accelerated, steady state mass removal. The existence of this incubation period has been validated by several other studies [56, 64] The final period that is outlined by Springer is the steady state period where mass removal per surface area for increasing impacts per surface area follows a linear, steady state relationship.

Using this relationship, Springer developed a fatigue-based model [64] for predicting surface erosion using material properties and impact energy which has been widely cited amongst similar literature and provide a foundation for the development of many useful models. However, the literature does also suggest that the method developed by Springer may not be suitable for newer surface materials used in modern wind turbines [61]. Therefore, it can be said that the springer method is a fundamental part of many complex models but is perhaps too dated to be used solely for prediction of erosion through liquid impacts. The model is also highly sensitive to the Poisson ration [61], which is undesirable for a model of this type.

The work of Springer has led to many further predictive models and frameworks such as Lopez .'s LEE Rain Erosion Computational Framework [50] and these are often used estimate an erosion level that is then validated by experimental or CFD data. Lopez uses this in conjunction with a CFD model to estimate the erosion and its severity and then the CFD model to validate performance loss through erosion of the leading edge. Another study which has adopted a similar approach to Lopez, is Law [53] who created a numerical model for leading edge erosion based on the liquid impact erosion theory outlined by Springer. However, within this study it should be noted that the authors agreed that their model for predicting failure through degradation seemingly failed, despite achieving results that were largely congruent with the literature. Both authors also highlighted the use of the Miner rule as a limitation to the study. Therefore, it can be said that this model provides a useful base for more complex studies but should not be used as a sole method for predicting liquid erosion effects [14, 61].

2.5.3 Experimental Modelling of LEE

The literature shows that there have been many attempts to physically model a wind turbine blade and simulate LEE. This is often conducted using a whirling arm test rig, which simulates the effect of water droplets impacting a surface [72].

Figure 16 - Whirling Arm Test Apparatus [73]

These studies provide useful insight into comparison of relative erosion resistance but suffer from an intensive erosion area with a low reproducibility of results which suggests there is still developments to be made regarding the experimental research of LEE [75]. Despite this, Sareen produced an experimental study into LEE which and how the erosion impacted operational and aerodynamic performance which is widely cited amongst the literature for its clear categorisation criteria for the different erosion stages [9]. However, despite its wide use amongst the literature, the estimated range of values for increase in drag and the overall AEP loss seem slightly overestimated when compared to operational data from other studies [53] at 5-600% [9] and 5-25% respectively.

This apparatus can be used to identify the length of incubation periods for different coating materials when subject to varying conditions. This was exemplified in a study by Bech [74], which successfully investigated the effect of raindrop diameter on the incubation period of a topcoat an epoxy coating with the results suggesting that the incubation period is sensitive to the rainfall intensity. Another study which adopted the experimental approach to achieve some useful findings, which has been previously mentioned, was by Nash [56] who used a Rain Erosion Test (RET) rig to investigate the impact energies associated with the varying stages of erosion. The results of this approach will be used within this paper to develop a relationship between the end of the incubation period and the material failure.

Within the literature, it is apparent that experimental research is often used as validation for numerical or CFD methods [9, 50]. This has been used to validate the approximations used within the Springer model which has suggested that the model is relatively accurate but the results of the model cannot be directly applied to leading-edge protection systems [75]. However, when paired with some modified parameter from accelerated RET tests, the model can be used to analyse the erosion strength of materials [75].

2.5.4 Impact of LEE on Annual Energy Production

This section reviews the previous research into the relationship between LEE and the Annual Energy Production (AEP) of wind turbines. This section aims to develop an understanding of the expected losses of wind turbines for the different erosion stages. The section also aims to develop an understanding of when the AEP losses should begin, develop, and peak through comparing numerical, CFD, experimental and operational data.

Within the literature, there is a consensual understanding that the impact of LEE on AEP should fall between 1% for low levels of erosion and 5% [2, 15, 16, 27, 50, 53] for the most severe cases of LEE. However, amongst the different studies, the achieved values for AEP reduction as a result of LEE is large, with studies estimating that 73% of the AEP could be lost due to LEE. In a study into impact of rain erosion on the leading edge, H. Law. estimated that medium levels of LEE would result in an AEP loss of 1.8% and 4.9% [53] for medium and severe erosion respectively. This disagrees with another key piece of research into the impacts of LEE on AEP by Sareen [9] which estimated that small amounts of leading-edge erosion can result in a 5% AEP loss, with the more severe cases of LEE resulting in a 25% AEP loss. Law does comment that their analysis does not consider the impact of solid airborne particles or multiple particles in conjunction with each other, which are known to accelerate the propagation of LEE [53].

Han [16] also conducted a study into the effects of LEE on large wind turbines at high Reynolds numbers, achieving a range of AEP losses between 2% and 3.7%. The variance between the estimated AEP losses for these studies, highlights that the chosen approach for modelling leading edge erosion has a significant impact on the AEP loss value that is calculated. The wide range of results also highlights the difficulty and complexity associated with the accurate measurement and analysis of the impact of LEE on AEP. H. Law chose a numerical approach to achieve the values of 1.8% and 4.9%, whereas Sareen [9] opted for an experimental approach and Han [16] who used a CFD approach. As Sareen and Han incorporated the number of pits and gouges along with the level of delamination when analysing the blade surface, which may be the reason for the significantly larger range. It is possible to compare these results to a practical scenario using the case study by Lopez [50], which used a 5MW NREL aerofoil and extensive data from an operational wind farm to estimate an AEP loss of between 1.6% and 1.75%. Therefore, it can be said that the range of 1-25% is generally acceptable, but realistic values should fall within a range of around 1-5%. Both of these ranges are somewhat validated by the limited available operational data, with Vestas quoting severe blade contamination can reduce AEP by 10-13% [76].

Another method that is used within literature to analyse the impact of LEE on wind turbine blades, is to measure the change in the coefficients of Lift and Drag due to LEE. As the surface of the leading edge becomes rougher because of leading-edge erosion, the flow becomes turbulent sooner causing premature separation of the flow. In turn, the coefficient of lift (C_l) reduces and the coefficient of drag (C_d) increases. Like direct AEP loss, there is a wide range of achieved values for the influence of LEE on the coefficients of lift and drag for a given aerofoil. Ge conducted an analysis on the S809 aerofoil, and how the C_d and C_l are influenced by LEE. The study estimated that the C_d can increase by between 131-217% paired with a reduction in the maximum C_l of between 35-61%. This somewhat agrees with the work conducted by Sareen, who estimates that drag can increase massively matched with a drastic reduction in C_l.

However, the values estimated by Sareen are like the AEP loss values, which were higher than other studies. The C_d range is incredibly wide, at 6%-500% from light erosion to severe erosion [9]. This is commented on in the study as the author highlights that the 500% value is based on a linear erosion for the entire length of the leading edge, when the distribution of the erosion is variable in practice. Therefore, the acceptable range of increases in drag was selected to be 6-500% which agrees with most of the previous work. The acceptable range in lift decrease, would be the range from 25-61% in line with the findings from Ge and Herring. A table of the ranges of values from these studies can be seen in Table 3.

Table 3 - Change in lift and drag coefficients from [9, 16, 77, 78]

Author	ΔC_l **(%)**	ΔC_d **(%)**
Ge	35-61	131-217

Herring	25	20
Sareen	6-15	5-600
Han	53	314
Gaudern	4-6	49-86

2.6 Key findings and Gap Statement

LEE has been identified as a complex challenge to the development of the wind energy, both onshore and offshore. However, within the research there is a shortfall of frameworks that can fully assess the temporal impacts of leading-edge erosion from the aerodynamic implications to the AEP losses and financial implications. The review of the literature highlighted that previous work has often evaluated the impacts of LEE in isolation, whether it be the sole review of the aerodynamic impacts or the material behaviour of the coating materials. This results in useful findings for each individual aspect of LEE development but fails to provide an understanding of how these impacts influence each other over the operating lifetime of a turbine.

Much of the work shows that there are significant differences between the predicted impacts of LEE between approaches. This highlights that these approaches must be used together to create a comprehensive framework for analysing the impacts of LEE on the performance of wind turbines using surface roughness to model the eroded geometry. A gap in the literature was found in the analysis of wind turbines throughout the entirety of their operating lifespan of 25 years, with many studies analysing a much shorter timeframe. A gap was also identified within the literature to develop a model which can analyse the development and consequent impacts of LEE on the AEP and economic viability of wind projects for a wider range of erosion stages.

3.0 Aims and Objectives

3.1 Project Aims and Objectives

This project aims to develop the limited research on the effectiveness of using surface roughness as a method of modelling the impact of leading-edge erosion on aerodynamic and operational performance.

The results of this analysis aim to provide a framework that can quantify the losses in annual energy production because of leading-edge erosion and how these losses vary temporally due to greater exposure to airborne particles. To meet these aims, the following objectives were defined as follows:

O1 – Develop a CFD model of a wind turbine aerofoil with a clearly defined leading-edge to measure the impact of surface roughness on lift and drag coefficients for different angles of attack.

O2 – Develop a numerical model that converts the lift and drag coefficients into a power coefficient for different tip speed ratios for use within annual energy production calculations.

O3 – Develop a model for estimating how the severity of leading-edge erosion develops over time for different regions.

O4 – Estimate the loss of energy production because of leading edge erosion using weather data.

O5 – Investigate the financial implications of the reduced AEP on wind farm developers and operators.

O6 – Investigate the environmental impact of leading-edge erosion on the surrounding regions, both onshore and offshore.

4.0 Methodology

This section describes the chosen approach, numerical and theoretical modelling chosen to achieve the aims and objectives defined in Section 3.1. A flow diagram illustrating the different analyses conducted within this study is shown in Figure 17.

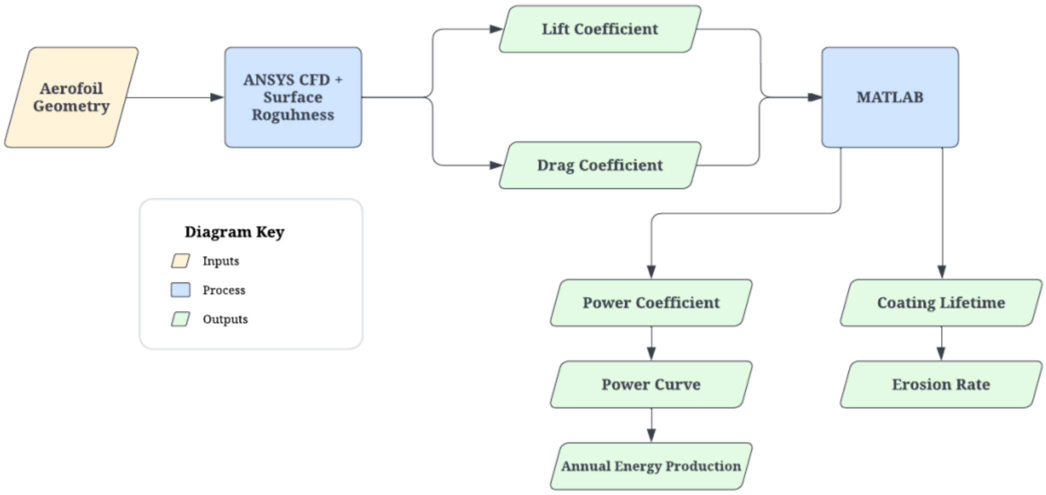

Figure 17 - Project flow diagram

4.1 CFD Aerofoil Model

To investigate the effect of LEE on the aerodynamic performance of wind turbine blades, a 2D model of a NACA 4412 aerofoil with a chord length of 1m was created in ANSYS Fluent. This model was used within a C-shaped structured mesh with dimensions shown in Figure 9, to analyse the flow behaviour over the aerofoil. The length of the mesh was set at 10 times the Chord Length (c) and the height was also set at 10c. The mesh was divided into three sections to increase the fineness of the mesh around the aerofoil.

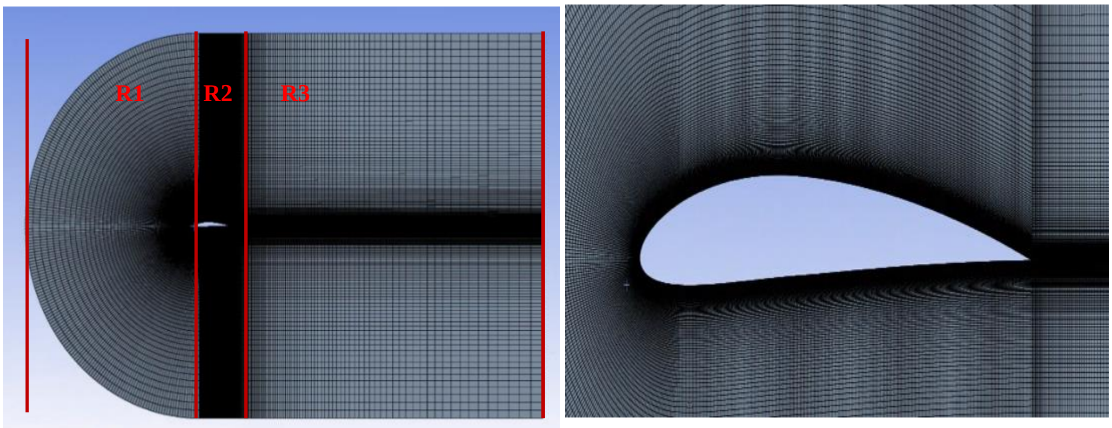

Figure 18 - ANSYS meshing geometry

Within the model geometry, the aerofoil was separated into two sections, the leading edge and trailing edge, using a named selection. This allowed for a surface roughness boundary condition to be created and applied to only the leading edge. The two regions are shown in Figures 19 and 20.

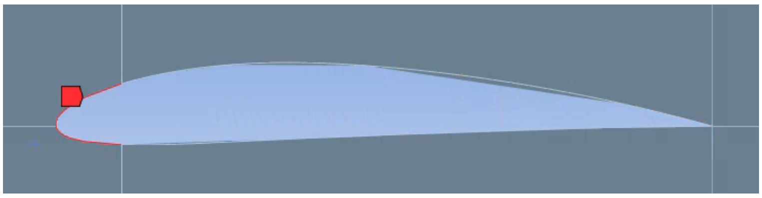

Figure 19 - Leading Edge Named Selection

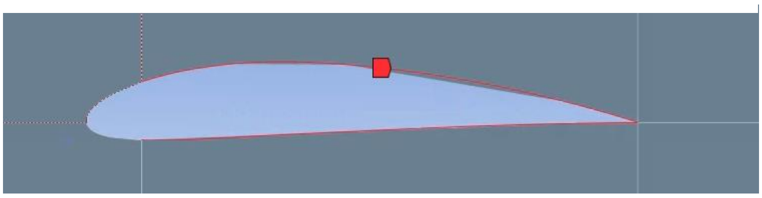

Figure 20 - Trailing Edge Named Selection

The Spalart Allmaras [79] viscous model was used within ANSYS as it has been experimentally validated as being capable of closely replicating the behaviour of the flow over a rough surface [70]. The LEE geometry was replicated using an equivalent sand-grain roughness boundary condition. The values for equivalent sand-grain roughness had been calculated successfully by Ravishankara [70] for Stage 3 and Stage 4 LEE and this approach was extended to calculate the equivalent sand grain roughness at stages 1 and 2 [71].

Firstly K_{rms} is computed using:

$$k_{rms} = \sqrt{\frac{1}{N}\sum_i {k_i}^2} \qquad (Eq.\ 1)$$

Where N is the total number of roughness elements and k_i is the roughness height of the individual elements. The skewness of the distribution is then calculated using:

$$Sk = \frac{1}{N}\sum_i \left(\frac{k_i}{k_{rms}}\right)^3 \; (Eq.\ 2)$$

Surfaces with pits and gouges are negatively skewed, the following relationship is used to calculate equivalent sand grain roughness, k_s.

$$k_s = 2.73 k_{rms}(2 + Sk)^{-0.45} \qquad (Eq.\ 3)$$

By selecting a Type 2A and 1A erosion from Sareen [9], k_s was calculated and used as a boundary condition within ANSYS Fluent. The boundary condition was applied to the leading-edge, and this was changed between simulations according to the different stages of erosion outlined in Table 4.

Table 4 - Erosion Stages and Equivalent Sand Grain Roughness

Erosion Stage	Equivalent Sand Grain Roughness (K_s/c)
0 (Clean)	0
1	0.0009
2	0.00129
3	0.00418 [70]
4	0.00760 [70]

To measure the effect of surface roughness, two monitors were used within ANSYS which would produce a plot of lift and drag coefficients for the set input parameters. The range of surface roughness was applied for varying AoAs to investigate the effect of these parameters on the lift and drag coefficient of the aerofoil. The AoA was changed between simulation by taking the sine and cosine of the AoA and using this as the X and Y components of the inlet flow. The angle was varied from 0-14 in two degree increments as shown in Table 5.

Table 5 - Inlet X and Y components for each AoA

AoA (°)	Inlet Y-Component	Inlet X-Component
0	0	0
2	0.0348995	0.99939083
4	0.06975647	0.99756405
6	0.10452846	0.9945219

8	0.1391731	0.99026807
10	0.17364817766	0.98480775301
12	0.20791169081	0.97814760073
14	0.2419218956	0.97029572627

The inlet velocity was set at 43.9 m/s which was chosen to produce a Reynolds number of roughly 3,000,000 to allow for the validation of the model's behaviour against previous studies [40].

4.2 Power Coefficient Model

To relate the computed lift and drag coefficients to the performance of a wind turbine, the following relationship was used to calculate a power coefficient as a function of tip speed ratio, number of blades and lift to drag ratio [80].

$$C_p = \frac{16}{27}\lambda\left[\lambda\frac{1.32+\left(\frac{\lambda-8}{20}\right)^2}{B^{\frac{2}{3}}}\right]^{-1} - \frac{(0.57)\lambda^2}{\frac{C_l}{C_d}\left(\lambda+\frac{1}{2B}\right)} \qquad \textit{(Eq. 4)}$$

Where:

λ = Tip Speed Ratio

C_l = Coefficient of Lift

C_d = Coefficient of Drag

B = Number of blades

Using this equation, a Power Coefficient could be calculated and used to estimate the annual energy production of a wind turbine and estimate the effect of LEE on the amount of energy that is produced.

4.3 Annual Energy Production Model

The Annual Energy Production (AEP) of a wind turbine is an important metric for wind farm developers and investors. Reductions in the AEP can have potential implications on the economic viability of wind farm projects. To estimate the AEP and any consequent reductions due to LEE, the following equation [81] was used:

$$AEP = \frac{1}{2} \times C_P \times \rho \times V^3 \times A_{rotor} \times Hours\ in\ operation \qquad (Eq.\ 5)$$

Where:

C_P = Power Coefficient

ρ = Density (kg/m^3)

V = Wind Speed (m/s)

A_{rotor} = Rotor Area (m^2)

Using the C_P model above, the clean blade was used as a baseline model to estimate the optimal energy production for the turbine blades. For each stage of leading-edge erosion, a new C_P is computed and a new AEP is estimated. For the V^3 parameter, a Weibull distribution is used to consider the variation of the local wind speed. The parameters for the wind turbine AEP calculation are as shown in Table 6.

Table 6 - Wind Turbine Specifications

Wind Turbine Specifications	
Rotor Diameter (m)	40
Cut-in speed (m/s)	4
Rated speed (m/s)	15
Cut-out speed (m/s)	25
Capacity Factor (%)	0.42

4.4 Estimation of coating lifetime and Erosion Rate

As mentioned within Section 2.2.1, the Springer model is a framework for estimating the effect on a surface because of a liquid droplet impact. As the stage of leading-edge erosion develops over time as more particle impacts occur, the Springer model was used to estimate the number of particle impacts until coating failure. Using this model to estimate the materials lifetime, the results of Nash's staged approach were used to estimate the number of impacts between the individual stages. Therefore, using both models, a surface roughness can be related to each erosion stage to estimate the AEP losses and the progression of the erosion stages over time.

4.4.1 Coating Lifetime Model

The coating lifetime model was developed from a study by Eisenberg and Hoksbergen. This study developed a Wind Turbine LEE Protection System Lifetime Model based on the principles of Springers rain erosion framework. These studies propose that the number of impacts upon a single location at a given impact velocity to cause failure of the blades coating, represented by ${N_i}^*$, is described as:

$$N_i{}^* = a_1 \left(\frac{\sigma_{e,s}}{\sigma_{0,s}}\right)^{5.7} \qquad \textit{(Eqn. 6)}$$

Where:

a_1 = Springer Constant

$\sigma_{e,s}$ = Substrate Erosion Strength

$\sigma_{0,s}$ = Substrate Stress

The model was set up with the following input parameters based on the material properties of a Topcoat blade coating which is often used in industry [2, 82, 83] to delay the onset of erosion. The material properties used within the model are shown in Table 10.

Table 7 - Coating material properties [61, 82, 83]

Coating Material Properties	
Coating Young's modulus [GPa]	3.81
Coating Poisson Ratio [-]	0.295
Coating density [kg/m3]	1690

Coating ultimate tensile strength [MPa]	13
Coating endurance limit [MPa]	6.31
Coating fatigue knee [-]	5.2
Coating thickness [m]	750e-6
Constants	
Liquid Density [kg/m3]	997
Liquid acoustic velocity [m/s]	1481
Impact velocity [m/s]	90
Droplet Diameter [mm]	1
Springer Constant, a1	7e-6
Springer Constant, a2	5.7

Hoksbergen [61] also showed that the $N_i *$, which is the number of impacts upon a single location, can be converted to the drops per metre-squared, N_i , based on the diameter of the impacting rain droplets [61]. The relationship between $N_i *$ calculated in Equation 6 and N_i is represented by the following equation:

$$N_i = N_i^* \frac{4}{\pi d^2} \qquad \textit{(Eqn. 7)}$$

Where:

N_i = Number of impacts per metre squared

N_i^* = Number of impacts upon a single location until failure

d = Droplet diameter (mm)

Therefore, the N_i value for the blade coating could be computed for a constant droplet diameter and once this number of impacts had been reached, the material was considered to have experienced total failure, indicating the end of the lifetime of the coating material.

4.4.2 Rainfall Rate Variation

The number of impacts is dependent on many meteorological factors, such as rainfall intensity and raindrop diameter, which have a direct impact on the number of impacts on the blade surface. Therefore, to estimate a realistic value for the damage rate, MIDAS data was used for four separate regions. Using the erosion maps developed by Stack [52] and MetOffice weather station data, it was possible to investigate the variation in erosion rate between different regions. An example of the MIDAS data used within the analysis can be seen in Table 11.

Table 8 - Sample Rainfall Data from MIDAS

Region	Hours of Rainfall	Rainfall range (mm/hr)	Avg. Intensity (mm/hr)
Aberdeen	1261	0.2-26.2	1.171

4.4.3 Raindrop characteristics

The terminal velocity of the raindrop is also dependent on the diameter of the raindrop through the following relationship developed by Atlas [84].

$$V_{terminal} = 9.65 - (10.3 \times e^{(-0.6 \times D_{raindrop})}) \qquad \textit{(Eqn. 8)}$$

Where:

$D_{raindrop}$ = Raindrop diameter in millimetres (mm)

For the calculation of terminal velocity $V_{terminal}$ will be computed for a constant raindrop diameter of 1mm, to allow for consistency between the raindrop diameter used in the coating lifetime model. To justify this raindrop diameter, the cumulative distribution function of droplet diameters as a function of rain intensity [85] was computed to identify the percentage of the rainfall which would be 1mm in diameter using:

$$F = 1 - e^{-\left(\frac{d}{1.3 \times l^{0.232}}\right)^{2.25}}$$

Where:

l = Rainfall intensity (mm/hr)

d = Raindrop diameter (mm)

The probability of the droplet diameters of the falling raindrops at the UK's rainfall rate of 0.1244 was estimated to be 80.7% showing that a constant droplet diameter of 1mm is a fair assumption. The cumulative distribution function is shown in Figure 21.

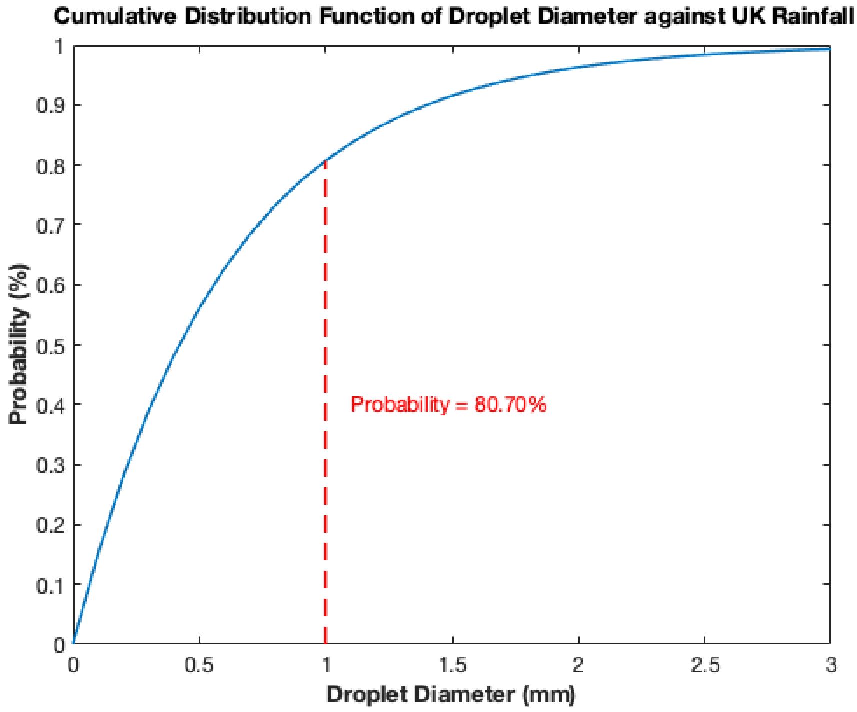

Figure 21 - Cumulative Distribution Function of Droplet Diameter

Therefore, using the constant droplet diameter of 1mm, the number of raindrops within a cubic meter of air can be described using the following relationship [2]:

$$q = 530.5 \times \frac{l}{V_{terminal} \times D_{raindrop}{}^{3}} \qquad \textit{(Eqn. 9)}$$

Where:

Q = raindrops per cubic meter

$V_{terminal}$ = Raindrop terminal velocity in m/s

$D_{raindrop}$ = Raindrop diameter in millimetres (mm)

l = Rainfall rate in (mm/hr)

As the turbine blade rotates, the impact velocity upon the blade will change. This impact velocity peaks at a rotation angle of 270 as the blade rotates upward, directly opposing the velocity of the rainfall, seen in Figure 22.

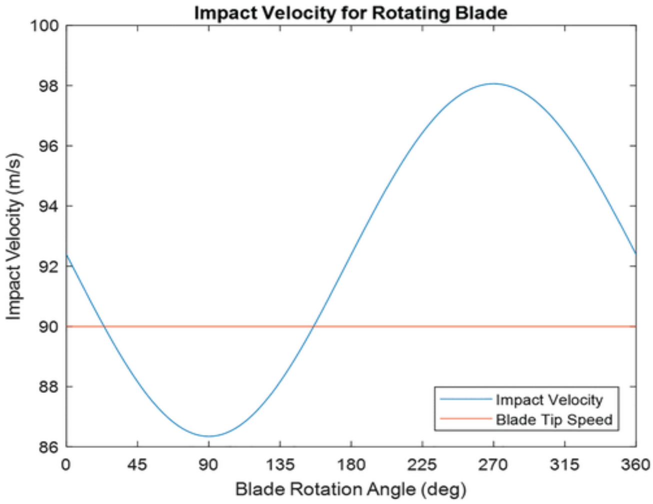

Figure 22 - Variation of impact velocity with Blade Orientation [53]

However, the assumption will be made that the impact velocity will be made constant and equal to the tip speed throughout the analysis to account for variations in the impact velocity throughout the period of operation. Despite the average across the rotation angle being higher than the tip speed, this is an assumption which has been used successfully in several other studies [53, 86]

The number of rain droplet impacts per metre squared is described using the following relationship:

$$\dot{N} = q \cdot V_s \cdot \beta(d) \qquad \textit{(Eqn. 10)}$$

Where:

$\dot{N}$ = Raindrop impact rate per m^2 per second

V_s = Impact velocity in metres per second

$\beta(d)$ = Impingement efficiency

Impingement efficiency, $\beta(d)$, is a variable which is dependent on raindrop diameter and the surface geometry. It represents the number of droplets that will impact the surface, described by the following relationship [87]:

$$\beta(d) = 1 - e^{-15D_{raindrop}} \quad \textit{(Eqn. 11)}$$

Using the $\dot{N}$ calculated in Equation 10 and the N_i calculated using Equation 7, the damage rate, D_i, per year can be calculated. From this, failure is achieved when the sum is equal to 1 of these damage rates is equal to one and this assumed as the lifespan of the turbine blade coating until failure.

$$D_i = \sum \frac{\dot{N}}{N_i} \qquad \textit{(Eqn. 12)}$$

Therefore, the damage rate and lifetime of the coating material can be expressed as:

$$Lifetime = \frac{1}{D_i} \qquad \textit{(Eqn. 13)}$$

Using the Staged Approach by Nash, it was observed that 78.7% of the energy required to reach material failure was used to reach the end of the incubation period. Assuming each rain droplet transfers the same amount of energy to the blade surface, the length of the incubation period is then equal to:

$$Incubation\ period = 0.787 \times \left(\frac{1}{D_i}\right) \qquad \textit{(Eqn. 14)}$$

5.0 Results and Discussion

5.1 Baseline Model

The clean blade model behaved as expected, showing an increasing C_l for an increasing AoA [34, 35, 41]. With increasing AoA, C_d also increased as expected [34, 35, 41].

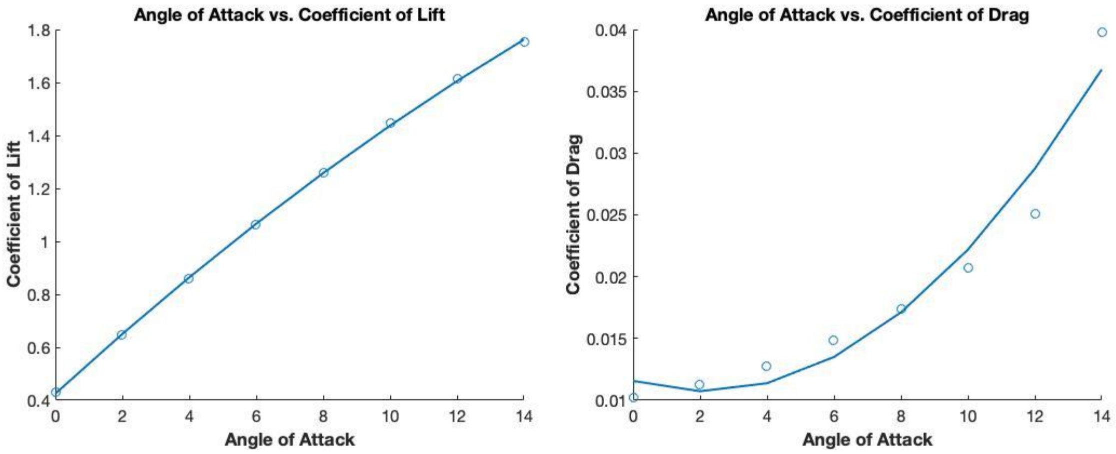

Figure 23 - Coefficients of Lift (Left) and Drag (Right) vs Angle of Attack

The peak value of C_l observed for the clean blade, was 1.75 matched with a C_d of 0.040 at 14 degrees AoA. However, the C_d that was estimated for a 14-degree AoA disagreed was shown to be an outlier to the previous data points. This was attributed to the fact that the stall angle of the aerofoil was 14-degrees, at which there is a change in the aerodynamic flow regime and a considerable reduction in aerodynamic performance.

As these results served as a benchmark for the roughened models, the model was validated against the NASA values for the NACA 4412. At an AoA of 13.87 degrees, NASA estimated C_l and drag to be 1.721 and 0.02861 [88], which closely matches the results of the model used within this study, which produced outputs of 1.7458 and 0.0324, for C_l and C_d respectively. The difference between the ANSYS model and the NASA values which were processed using CFL3D and FUN3D can be seen in Table 12.

Table 9 - Baseline model vs NASA values

FUN3D		CFL3D	
$\Delta\ C_l$ (%)	1.67	**$\Delta\ C_l$ (%)**	1.44
$\Delta\ C_d$ (%)	9.94	**$\Delta\ C_d$ (%)**	13.24

Comparing the NASA results to the ANSYS results, the ANSYS values are within 2% of the published values, suggesting that the ANSYS model is capable of accurately estimating the coefficient of lift. However, the model seems to overestimate the drag value with an average 12% percentage error against the NASA values processed using FUN3D and CFL3D.

5.2 Aerodynamic Impact of Leading-Edge Erosion

The model was run for the range of surface roughness's and the increasing angles of attack up until the stall angle. The relationship between the increasing AoA and the computed lift and drag coefficients can be seen in Figure 24.

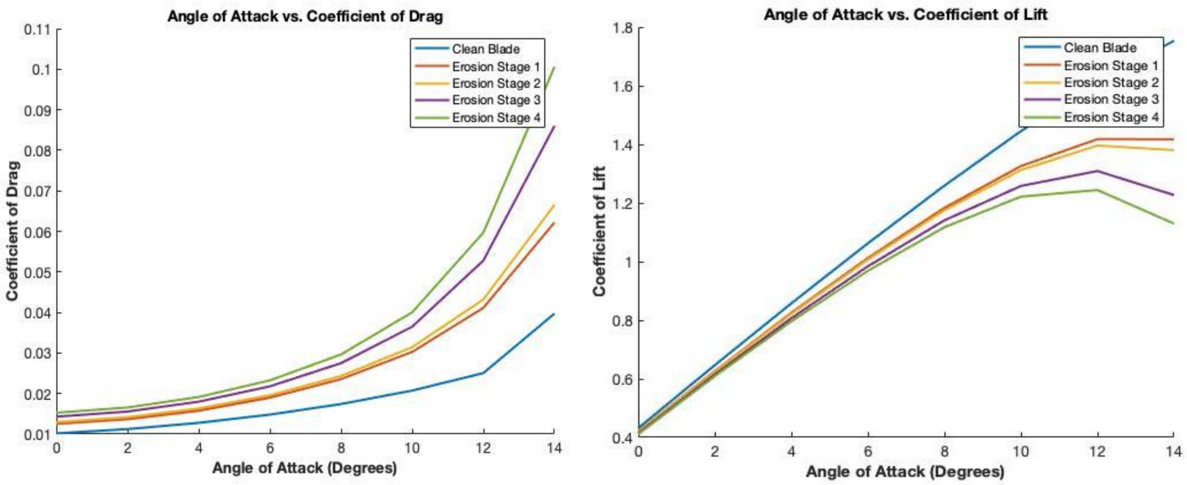

Figure 24 - Coefficients of Drag (Left) and Lift (Right) for Clean and Eroded Blades

The model behaves as expected, with C_l decreasing with increased surface roughness and C_d increasing with surface roughness at each AoA. This is due to the increased surface roughness around the leading causing a premature separation of the flow from the upper side of the blade. The drag also increases with AoA as the area of the aerofoil directly facing the freestream airflow increases, generating increased drag but significantly greater lift. The clean blade also demonstrates considerably lower values of drag and significantly greater values of lift when compared to stage one erosion. This suggests that the presence of any roughness on the surface of the blades has a significant impact of the flow behaviour when compared to a clean blade.

Figure 12 shows that the C_l increases for all angles of attack in the case of the clean blade. However, for the eroded cases, C_l peaks at a 12-degree AoA before slightly decreasing in the case of stage one and two erosions. For the more severe erosion stages, the decrease in lift beyond a 12-degree AoA is far more significant. These results suggest that leading edge erosion has a greater impact at higher angles of attack, with drag significantly increasing at higher angles of attack matched with a decrease in lift for the eroded cases.

To further visualise the relationship between lift, drag and surface roughness the values of lift-to-drag ratio were plotted for each AoA. The lift-to-drag ratio results show that the lift-to-drag ratio is most optimal at an AoA of 8-degrees for the clean blade. For the eroded simulations, the peak lift-to-drag ratio occurred at a 6-degree AoA showing that the optimal AoA for lift generation and drag minimisation has shifted due to LEE. The lift-to-drag ratio plot is shown in Figure 25.

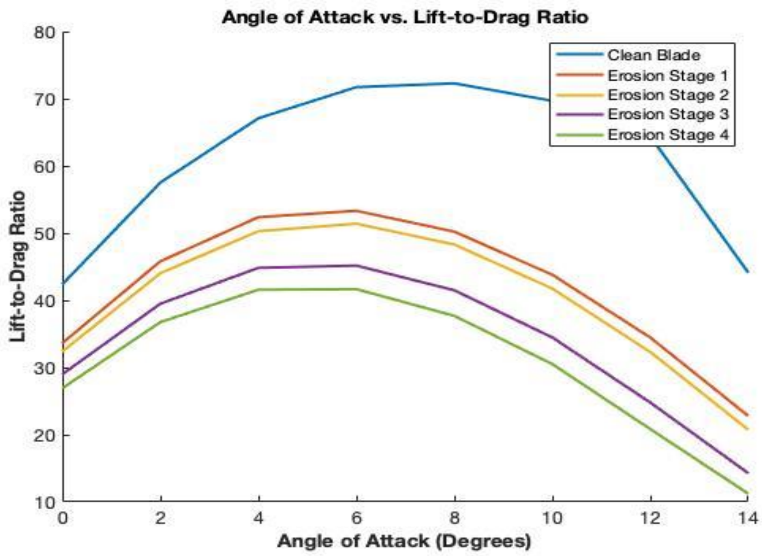

Figure 25 - Lift to Drag ratio vs AoA

The lift-to-drag ratio also validates that leading edge erosion has a significant influence on the aerodynamic performance. For all stages of erosion and angles of attack, the computed lift-to-drag values are significantly lower in comparison to the clean blade. The values of lift-to-drag show that there is a significant drop in performance for all stages of erosion beyond an 8-degree AoA. The trends show that the presence of leading-edge erosion have a significant impact when compared to a clean blade with no roughness. This impact is then most significant between stages 2 and 3 as the surface roughness used within the model increases significantly between these stages. The peak value of lift to drag is 72.28 and occurs at 8 degrees for the clean blade. For all cases of eroded surfaces, the peak value of lift to drag occurs at an AoA of 6 degrees, suggesting that the presence of leading-edge erosion has a potential impact on the optimal lift-to-drag generation for wind turbine blades.

5.2.1 Aerodynamic impact validation

5.2.1.1 Baseline model validation

The baseline model used for comparison to the NASA simulations for lift and drag showed that the model is accurately estimating lift to within 1.5% error. However, the model showed a slight overestimation in the C_d at around 10% percentage error. This disparity can be attributed to the fact that the Reynolds number used within the baseline simulation was higher, at 3×10^6, to the Reynolds number used within the NASA simulations at 1.85×10^6. This produces discrepancy between the results as C_d is highly dependent on Reynolds number [40] and this can be recognised as the reason for the percentage error between the baseline model and the NASA values.

5.2.1.2 Lift-to-drag validation

The results of the simulations show that an AoA of 8-degrees produces the greatest lift to drag ratio, suggesting this is the optimal AoA for the chosen aerofoil and operating conditions. The results of the simulations also agree with Kevadiya , who concluded that the lift-to-drag ratio for the NACA4412 increases with AoA up to 8 degrees [34]. The study also concluded that beyond 8 degrees, the ratio of lift to drag decreases for the NACA4412 aerofoil. The stall angle, 14 degrees, was shown to produce the lowest lift-to-drag ratio. This is supported by Petinrin [41], who concludes that the stall angle for the NAC4412 aerofoil is 14 degrees for all Reynolds number ranges between 1×10^6 and 13×10^6 [41].

However, although the trends for lift, lift-to-drag are largely congruent with the literature, there were some slight differences between the published values and the output of the model. The peak value of lift-to-drag for the clean blade was lower than the published values for the NACA4412. The peak value of lift to drag observed within this study was 72.28 whereas the peak value observed for NACA 4412 by Klritbhai [35] was 102.92. However, these studies are not directly comparable due to the difference in freestream velocities between the two studies. This discrepancy can also be attributed to the overestimation in C_d due to the higher Reynolds number used within the simulations as the C_l is not as dependent on the Reynolds number [40].

5.2.1.3 Decrease in C_l validation

The decrease in lift was estimated to be between 2.48% and 35.16% for the range of erosion stages and angles of attack. This result largely aligns with the previous work within the field as it is within the range of published values. A comparison between the ranges of decrease in lift due to LEE from previous studies is shown in Figure 26.

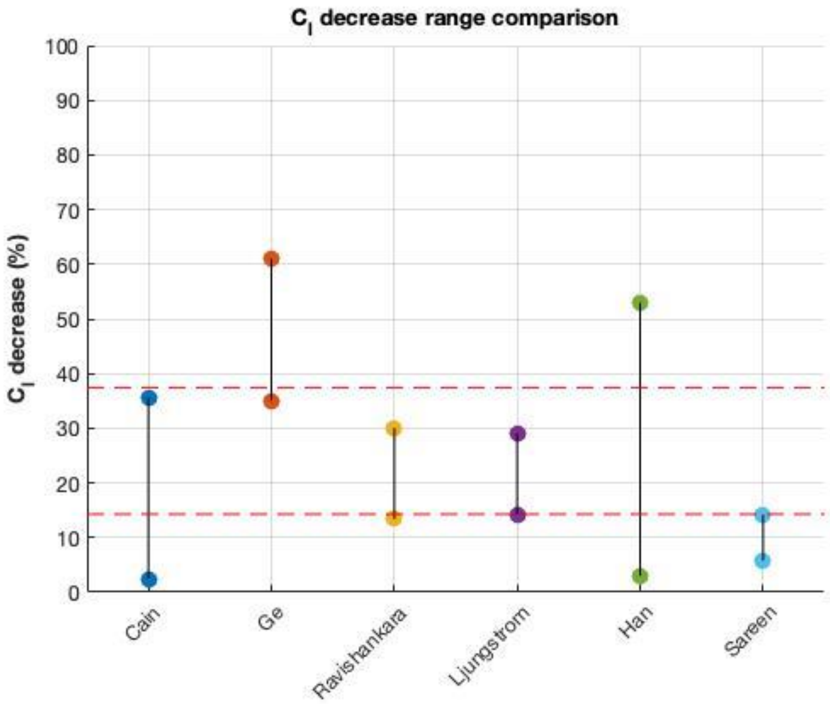

Figure 26 – Range of decrease in $C_l$comparison

The results of this study showed a slightly wider range of values than Ravishankara [70], Ljungstrom [70] and Sareen [9]. This can be attributed to both the larger Reynolds Number used within this study and the range of different AoA's and erosion stages used. The results of Han show a wider range of results whilst using a similar approach, which suggests analysing the impact of LEE on C_d using this approach leads to a larger range of values. The discrepancy between the results of this study and the study by Han can be attributed to the different equivalent sand grain roughness values used within the studies.

Overall, the range of decrease in C_l because of LEE agrees with the previous studies, aligning just out with the median range of values observed in previous studies. The results also show that change in C_l for lower erosion stages may be underestimated using this approach, as they fall out with the lower bound of the median range of values. However, as the different studies define the erosion stages differently, it is difficult to understand the cause of this underestimation.

5.2.1.4 Increase in C_d validation

The results for the increase in C_d were found to be align with the ranges estimated by previous studies. A comparison between these ranges is shown in Figure 27.

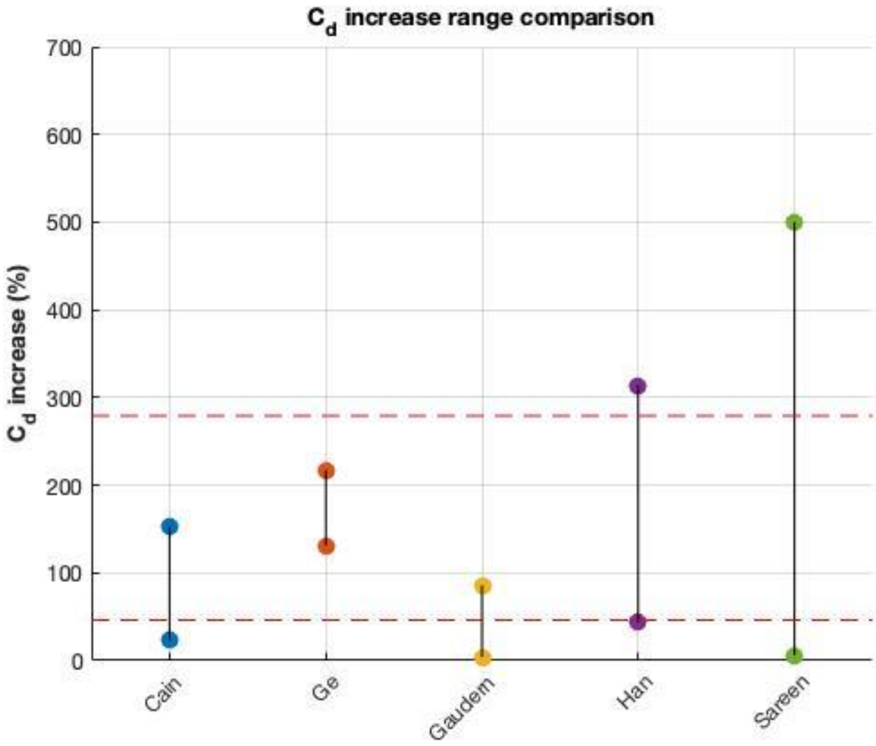

Figure 27 – Range of C_d increase comparison

The comparison between the results of this study and the previous studies show that the impact of LEE on the aerodynamic performance of wind turbine blades is significant, however, the severity of the impact is highly dependent on the chosen modelling approach.

Upon comparison to the results of Sareen, the range is far narrower suggesting that there is a discrepancy between the two studies at some stage during the modelling approach. This can potentially be attributed to the fact that Sareen considered all types of each erosion stage, A, B, and C which includes delamination whereas this study only considered Type A for each erosion stage. However, upon comparison between Sareen the median range, the upper range of values from Sareen are significantly greater than the other studies. Furthermore, the peak value observed by Sareen is over 300% larger than the peak value observed in this study, suggesting that the peak value by Sareen may be overestimated. Ultimately, the results do agree with literature as the values for the change in drag fall within the median range of the other studies with the exception of a slight underestimation of drag which may be caused by the lower value of Cd increase observed by Ge skewing the lower bound of the median range.

5.3 Impact of LEE on Annual Energy Production

5.3.1 Power coefficient

Figures 28-31 show the variation of Cp with TSR for each AoA and surface roughness. Assuming that annual energy production is estimated using the maximum achievable power coefficient, the impact on energy production due to leading-edge erosion could be estimated.

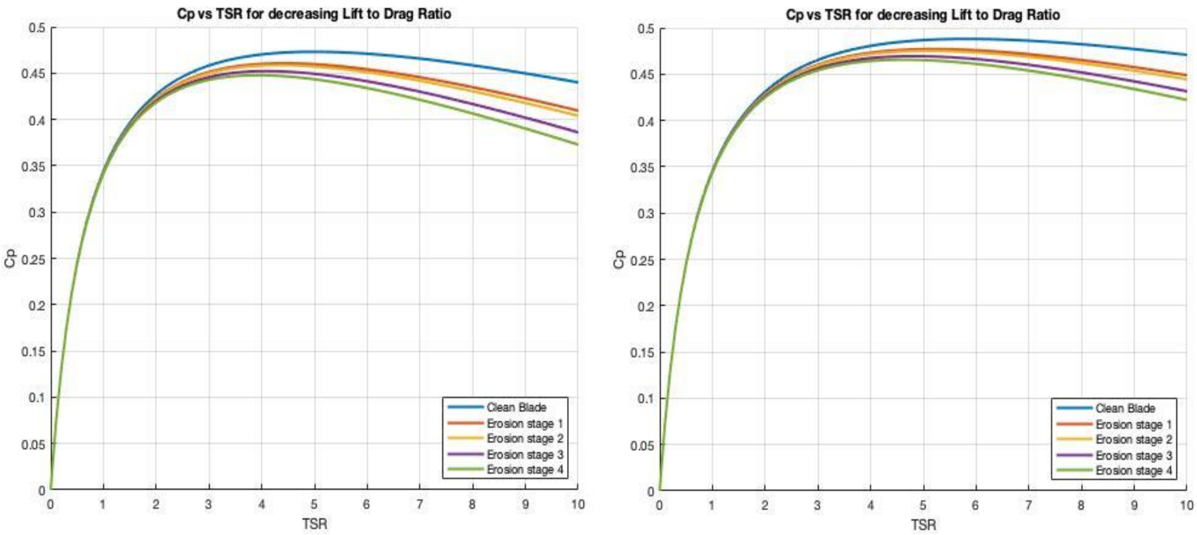

Figure 28 CP vs TSR for 0 (left) and 2 (right) AoA

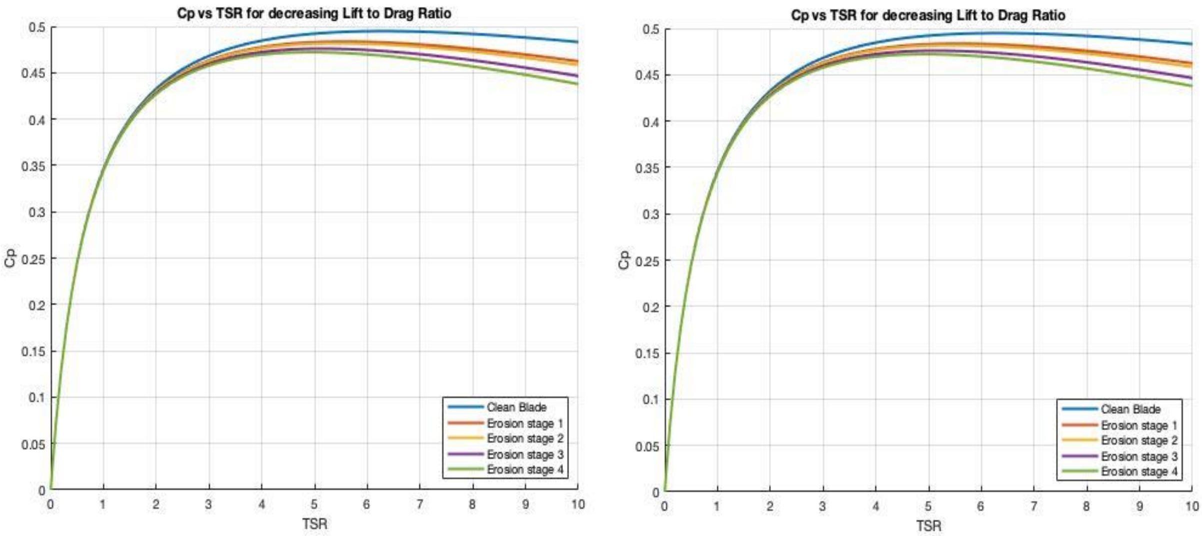

Figure 29 - CP vs TSR for 4 (left) and 6 (right) degree AoA

For an AoA of zero, the maximum achievable Cp is the lowest, due to this being the AoA which produces the lowest lift to drag ratio. For low angles of attack, the difference in the maximum achievable Cp for the eroded surfaces is small. Between 2- and 6-degrees AoA, the difference between the maximum achievable cp for the eroded blades and the clean blades is relatively small, with the values of Cp falling within a range of 0.448-0.498 with these Cp's occurring at the ideal operating tip speed ratios for wind turbines which is between 5-7 [89, 90].

However, figures 1 and 2 show that the Cp's begin to reduce beyond a TSR of 6. This disagrees with the typical ideal operating conditions of wind turbines in industry today, which is between 6-8 [89, 90].

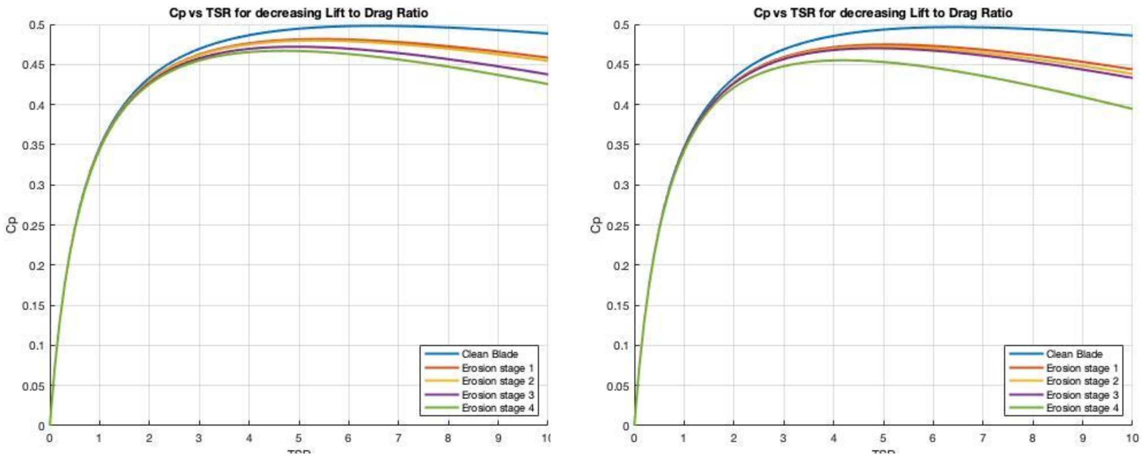

Figure 31 - Cp vs TSR for 8 (left) and 10 (right) AoA

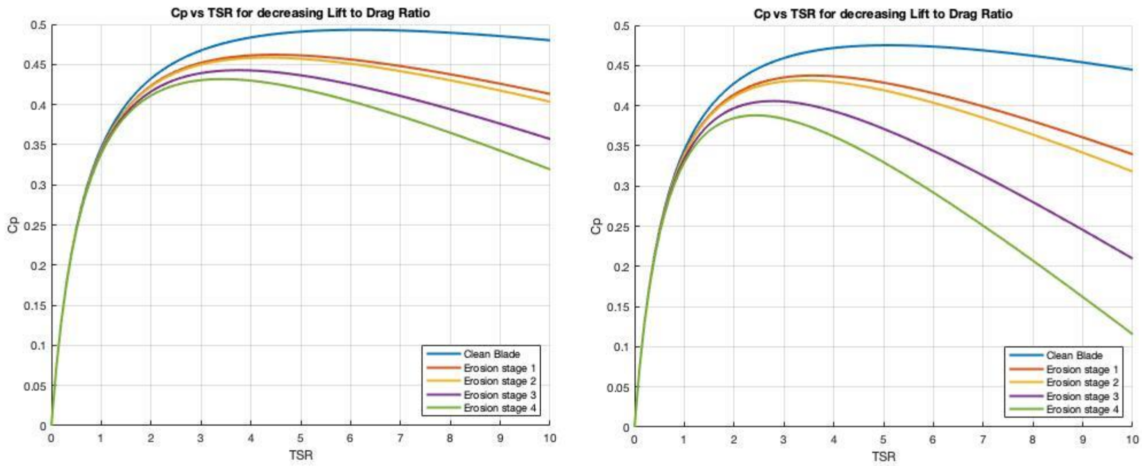

Figure 30 - Cp vs TSR for 12 (left) and 14 (right) AoA

The observed Cp's for an 8-degree AoA (Figure 4) show similar trends to Figures 2 and 3, with the eroded surfaces having a slightly smaller maximum achievable Cp than the clean blade for TSRs greater than 2. However, beyond a 10-degree AoA, the separation between the trend lines for the eroded surface grows significantly. This observation is supported by the maximum achievable Cp for these four angles of attack. For an 8-degree AoA, the clean blade achieved a Cp of 0.498, and this reduced to 0.467 which is a 6.42% reduction in Cp for the most severe stage of erosion. The reduction in Cp between the clean blade and the most severe stage of erosion is greater at a 10-degree AoA, with the clean blade achieving a Cp of 0.496 which reduced by 8.62% to 0.455.

For a 12-degree AoA, the clean blade achieved a Cp of 0.493 and this was reduced to 0.432 for the most severe level of erosion, which is a 13.19% decrease. For a 14-degree AoA, the clean blade achieved a lower Cp of 0.475 and this reduced to 0.388 for the most severe stage of erosion which is a 20.16% reduction in Cp. Therefore, it can be said that with increasing AoA and increasing stage of erosion, the coefficient of power reduces.

Furthermore, it can be seen from the graphs that the TSR at which the optimal Cp is achieved reduces and at a high enough AoA, falls out with the ideal operating TSR range of turbines in operation today [89] for the higher angles of attack. The maximum achievable Cp values for each stage of erosion and AoA are closely correlated with the lift-to-drag relationship as Equation 4, shown in Section 4.2, is a function of TSR, number of blades and lift-to-drag ratio.

5.3.2 Power coefficient validation

The results of the Power coefficient plots are useful as they relate the impact of LEE on aerodynamic performance to the impact on operational performance. The relationship used to compute the power coefficients, was for the maximum achievable power coefficient which suggests there may be a slight overestimation in the computed values for power coefficient within the analysis. Despite this, the range of computed power coefficients fell within the range of power coefficients observed in wind turbines today, suggesting that the model is capable of accurately estimating the power coefficient from the lift and drag characteristics of the chosen aerofoil.

However, the varied TSR used within the power coefficient calculations, would have an impact on the freestream velocity used within in ANSYS which was not accounted for within this study. As TSR is increased for a constant diameter, in theory, the freestream velocity used within the ANSYS simulation should increase to account for this change in TSR. Furthermore, with the varying freestream velocities, the Reynolds number of the flow would change which may have had an impact on the results. This can be recognised as a limitation of the study as the results may vary significantly with a changing TSR.

5.3.3 Power curve

The power curves of the aerofoil were plotted for each surface roughness and AoA to visualise their impact on the capacity of a given turbine. The results showed that the impact of leading-edge erosion is independent of the turbine diameter. Therefore, the results shown in Figures 25-28 were based on a 40m diameter turbine.

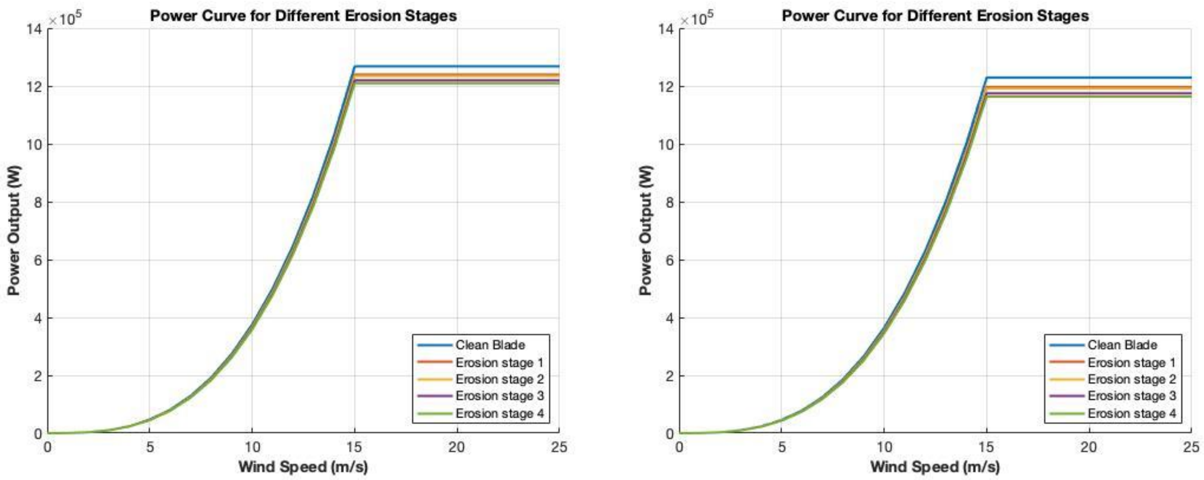

Figure 32 - Power curves for eroded blades and 0 & 2 degrees AoA

For 0-2 degrees AoA, the power output at the rated wind speed is reduced for all stages of erosion. The reduction is minimal between the stages, with the most severe stage of erosion causing a reduction in rated power output of 5.5% and 4.7% for 0- and 2-degrees AoA respectively.

For 4-6 degrees AoA, the power output at the rated speed is also reduced for all stages of erosion. The resulting power curves are shown in Figure 28.

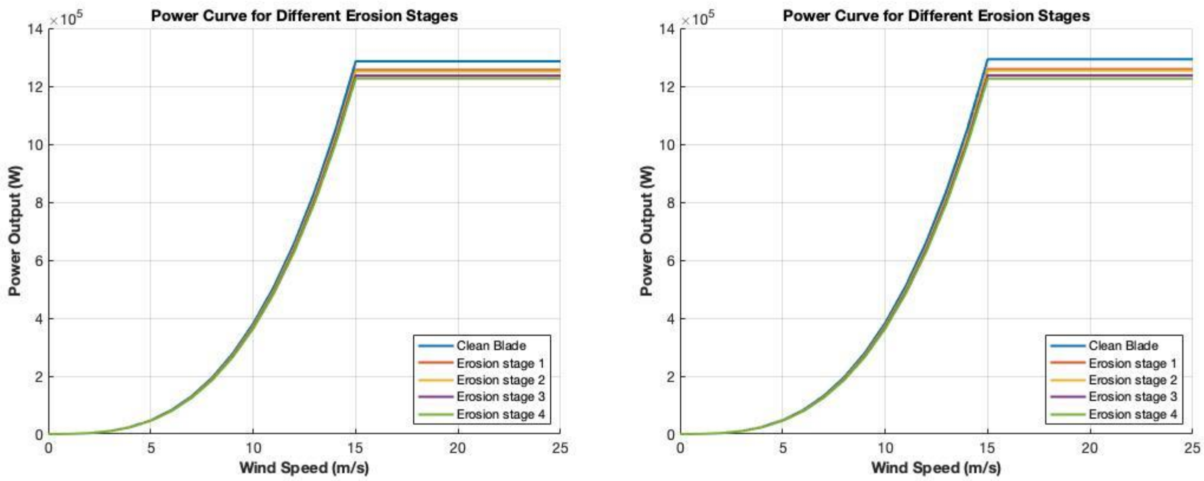

Figure 33 - Power curve for eroded blades at 4- & 6-degrees angle of attack

For the most severe stage of erosion, the reduction in rated capacity is 4.7% at 4 degrees AoA and 5.29% at 6 degrees AoA. This shows that for ranges of low AoA, 0-6 degrees, the greatest reduction in rated capacity due to leading edge erosion is erosion occurs at 0 degrees. However, beyond this angle the rated capacity reductions increase with AoA.

For 8- and 10-degree angles of attack, the reductions are slightly more noticeable on the power curves seen in Figure 29.

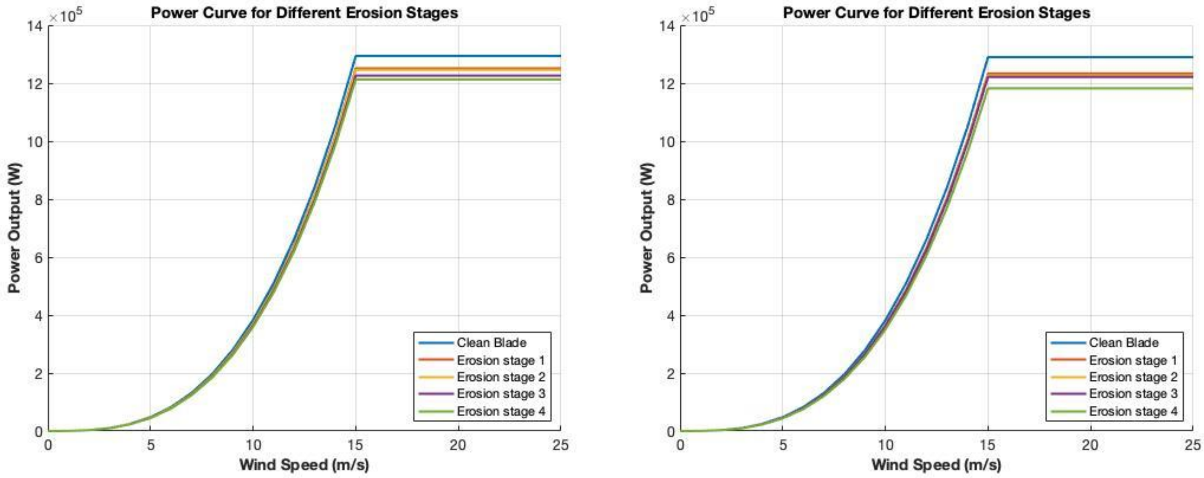

Figure 34 - Power curves for eroded blades at 8 & 10 degrees AoA

At an 8-degree AoA, the power curve shows a 6.4% reduction in rated capacity at the most severe stage of erosion. Furthermore, the reduction in capacity between the clean blade and stage 1 erosion has increased significantly. At a 10-degree AoA, the reduction in rated capacity at the most severe stage of erosion is 8.69%. At this AoA, the rated capacity drops dramatically for the first erosion stage followed by a minimal change between stages 2 and 3. Finally, there is another significant reduction in capacity when stage 4 erosion develops.

For the highest angles of attack, 12 and 14, each stage of erosion resulted in a significant reduction in rated capacity.

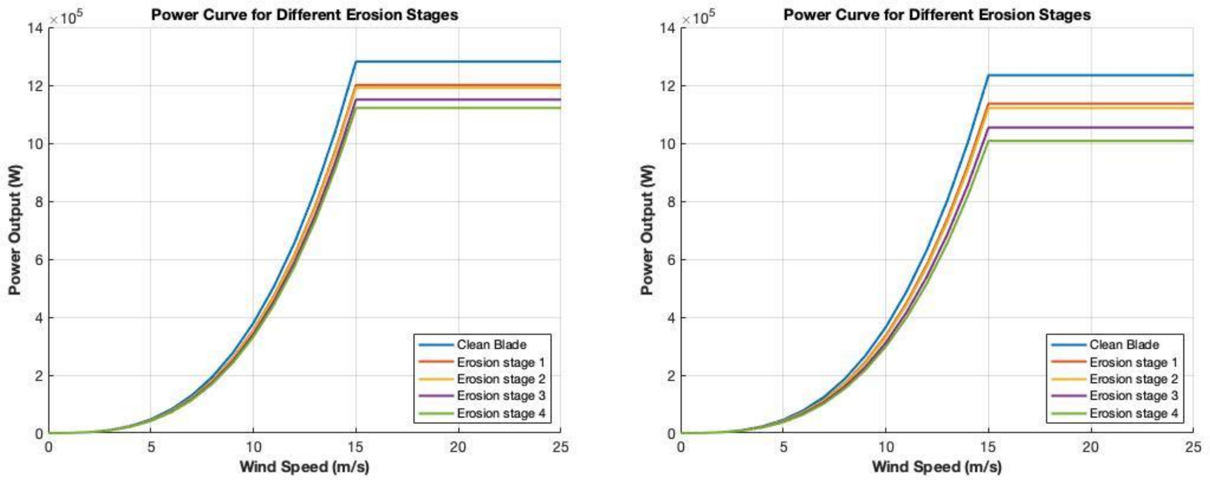

Figure 35 - Power curves for eroded blades at 12 & 14 degrees AoA

Figure 28 showed that for a 12-degree AoA, Stage one erosion resulted in a 6.5% reduction in rated capacity which is a greater consequential reduction than the most severe stage of erosion at all angles of attack between 0- and 8-degrees. Stage 4 erosion at this AoA resulted in a reduction in rated capacity of 13.26%.

The right-hand side of Figure 28 shows that for a 14-degree AoA, the presence of stage one erosion on the surface of the blade will cause an 8.26% reduction in rated capacity, which is a larger consequential reduction than the most severe stage of erosion for all angles of attack between 0 and 10. Stage 4 erosion at this AoA caused a significant reduction in rated capacity at over 20%.

The power curves further highlight that the effects of leading-edge erosion are far more significant at higher angles of attack. The results of the power curves contextualise the aerodynamic impact of leading-edge erosion outlined in Section 5.2 within the context of rated power production.

5.4 Annual Energy Production Losses

The results of the annual energy production calculations for both the clean and eroded blades agree with the previous findings on the power curve and power coefficient, showing decreasing annual energy production for increasing erosion stage. This consistency indicates that the calculations are reliable and that the energy production estimations are accurate for both blade types. These findings support the validity of the methodology used and provide confidence in the projected energy production for the given wind turbine system.

5.4.1 Angles of Attack 0-6 degrees

The AEP calculations for the lower angles of attack, between 0 and 6, show a notable difference in AEP because of LEE for all stages. Furthermore, the validity of the methodology is supported as the trend of increased loss at increasing angles of attack is demonstrated in Figures 22 and 23.

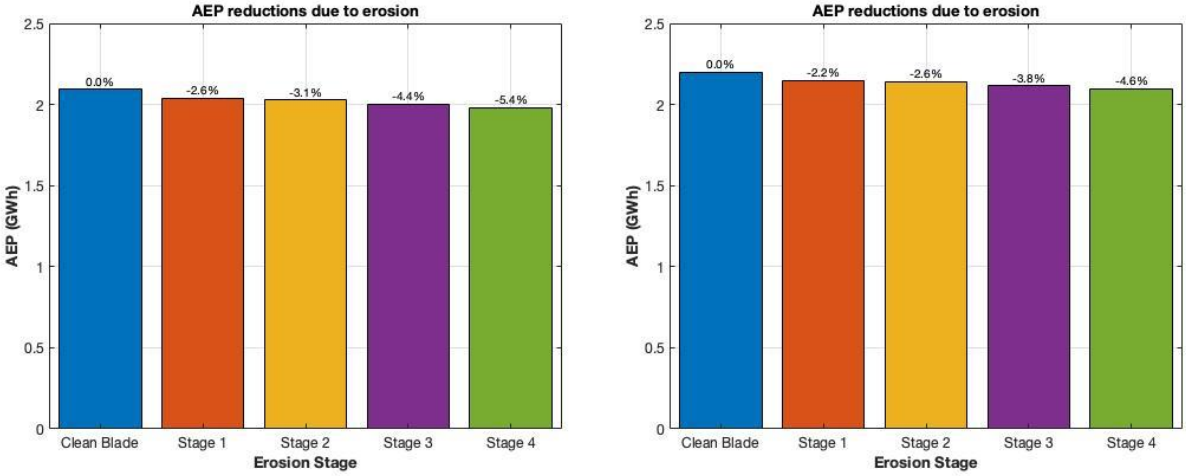

Figure 36 - AEP reductions for 0- and 2-degree AoA

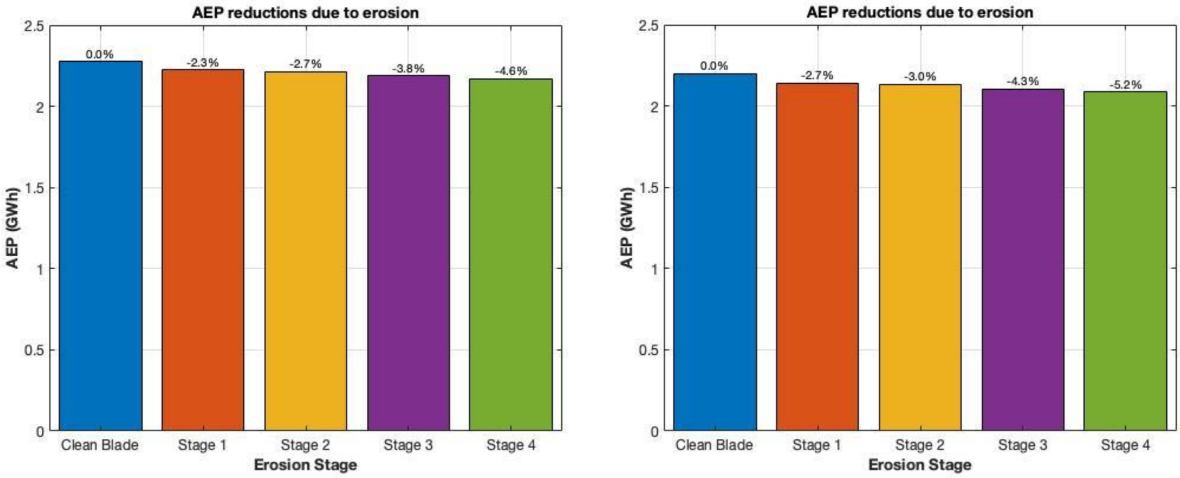

Figure 37 - AEP reductions for 4- and 6-degree AoA

At a 0-degree AoA, the largest change in AEP can be observed at Stage 1, which shows a 2.6% change from the previous stage being the clean blade. Between stages 1 and 2 the AEP decreases by 0.5%, followed by a further decrease of 1.3% when the erosion develops to stage 3. The most severe stage of erosion results in a 5.4% AEP reduction.

For a 2-degree AoA, the reductions in AEP between the individual stages and the total reduction from a clean blade to stage 4 erosion is lower than what was seen for the 0-degree

AoA. This agrees with the reductions in power curve which also highlighted a lower reduction at 0-degree AoA with an increase in reduction thereafter.

The reductions in AEP at a 4-degree AoA agree with the general trend of increasing losses with increased angles of attack beyond zero. However, these increased losses only occur for erosion stages 1 and 2, with no increase in AEP losses at stage 3 or 4 erosion.

At a 6-degree AoA, the observed AEP losses are greater than the losses observed at a 4-degree AoA for all erosion stages. The greatest increase occurs at stage 4 erosion which rose from 4.6% to 5.2% between the two attack angles.

5.4.2 Angles of Attack 8-14 degrees

In line with the previous findings, the losses at higher AoA's are far more significant for all stages of erosion. The AEP losses at each stage of erosion for the angles of attack between 8 and 14 degrees can be seen in Figures 24 and 25.

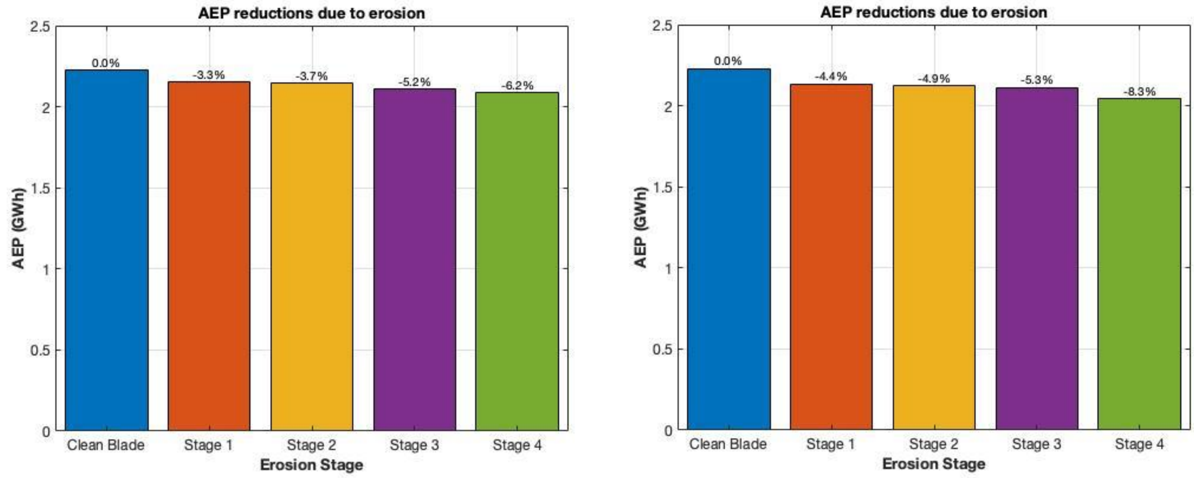

Figure 39 - AEP reductions for 8- & 10- degree AoA

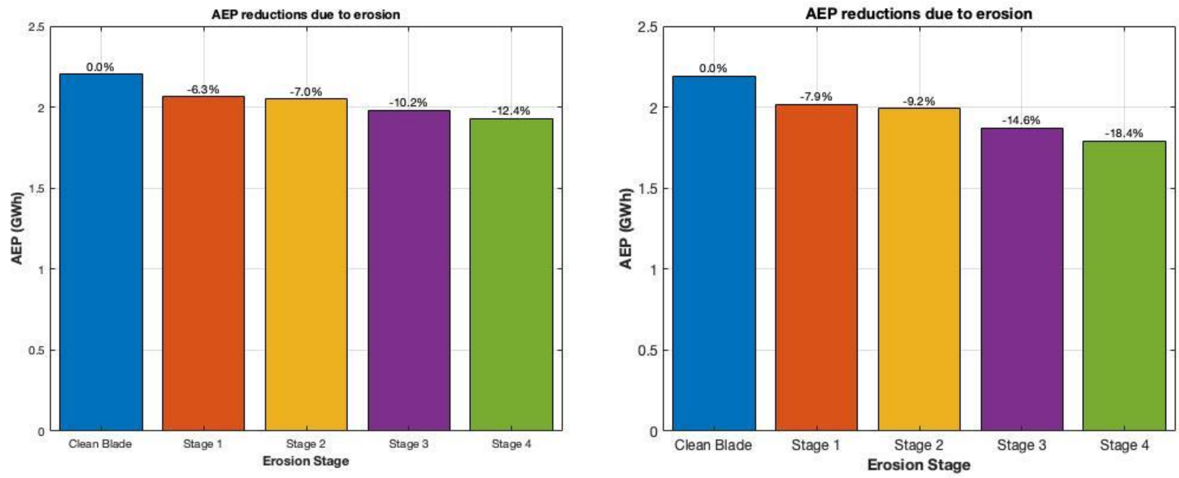

Figure 38 - AEP reductions at 12- & 14-degree AoA

At an attack angle of 8 degrees, the AEP losses are significant for each erosion stage. Once again, the stage that shows the greatest increase in AEP loss is stage 4 erosion showed a 6.2% decrease in AEP production against the clean blade. Furthermore, the difference between the clean blade and stage one erosion has decreased by 3.3%. An attack angle of 10 degrees continues to follow the trend of increased losses at increased angles of attack.

Furthermore, the erosion stage which is showing the greatest increase in AEP losses upon the previous stage, at 3%, is stage 4 erosion which is congruent with the trends observed for the previous angles of attack. At a 12-degree AoA, the losses in AEP due to leading edge erosion increase significantly. Losses at stage 1 have increased to 6.3% and Stage 2 to 7.0%, which is more than double the losses that were observed at a 6-degree attack angle for the same stage of erosion. Equally, stage 3 and 4 erosions have risen to 10.2% and 12.4% respectively. This agrees with the previous trends as the impacts of LEE at these higher angles of attack is being demonstrated through significant AEP losses. The final AoA, 14 degrees, shows very significant energy losses at all stages of erosion, peaking at 18.4% for stage 4 erosion.

5.4.3 Loss in AEP validation

The calculated AEP losses vary considerably with AoA. The most significant AEP loss was 18.4% observed at a 14-degree AoA and stage 4 erosion. This peak value fell within the range of expected losses outlined by Sareen and Wang [9, 17], but higher than the ranges observed in other studies [2, 15, 16, 26, 27]. A comparison between the maximum predicted AEP loss of each study is shown in Figure 40.

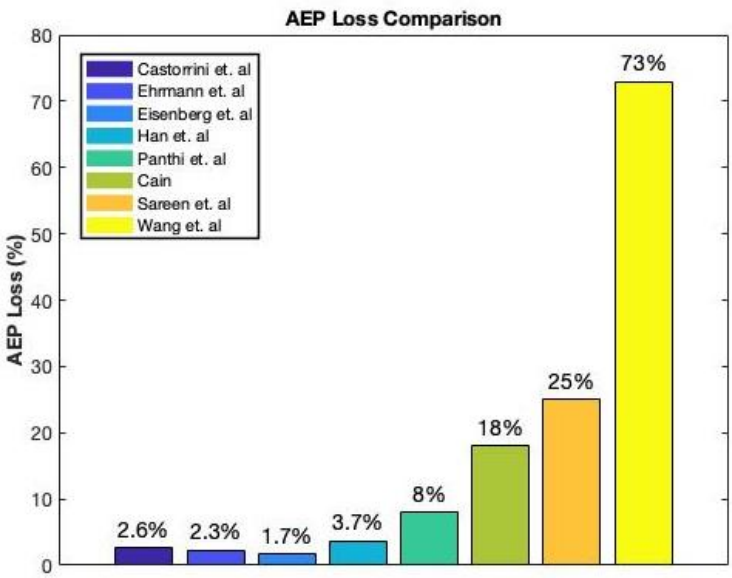

Figure 40 - AEP loss comparison with the literature values

The discrepancy between the results of the other studies with lower ranges and the results of this study, is because this study included the stall angle of the aerofoil within the analysis which has considerably higher drag and consequently a greater AEP loss. Despite this, the results of this study corroborate with the results of the previous studies, suggesting that the AEP losses calculated within this study are representative of the AEP losses that may be encountered in practice. The results also align with the results of Han [16], who recognised that the severity of AEP increased with erosion severity and AoA.

When considering the AEP losses for the most optimal AoA, 8 degrees, the AEP loss is estimated to be 6.2% which aligns much more closely to the lower range of values shown in Figure 38 [2, 53, 77] which are validated by operational data. This value of 6.2% also aligns much more closely to the target range of 1-5% outlined in the literature review.

Overall, the range of AEP losses estimated by this analysis are largely congruent with the literature. For the most optimal AoA, the AEP results corroborated with the results from both numerical and CFD models as well as operational data. Although, the variation in the observed ranges of lift-to-drag from the literature, make it difficult to fully compare the accuracy of this model to the literature.

5.5 Temporal Analysis of Leading-Edge Erosion Development

The temporal analysis of leading-edge erosion between stages is relatively unexplored within the existing literature. Therefore, temporal analysis was conducted to investigate the development of leading-edge erosion upon turbine when subject to varying rainfall intensities and frequencies over their operating lifespan.

5.5.1 Erosion progression and coating lifetimes

Figures 26 and 27 show the erosion progression against the time in years for the chosen four regions: Skye, Glasgow, Aberdeen, and Sheffield based on the developed erosion model outlined in Section 4.4.

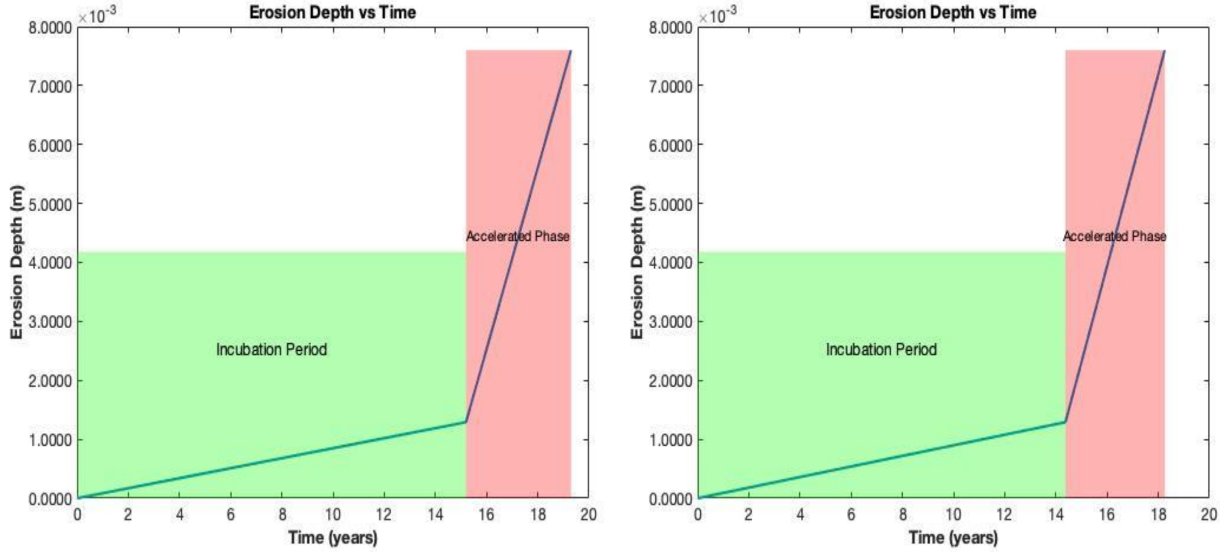

Figure 41 - Erosion Depth vs Time for Aberdeen (left) and Sheffield (right)

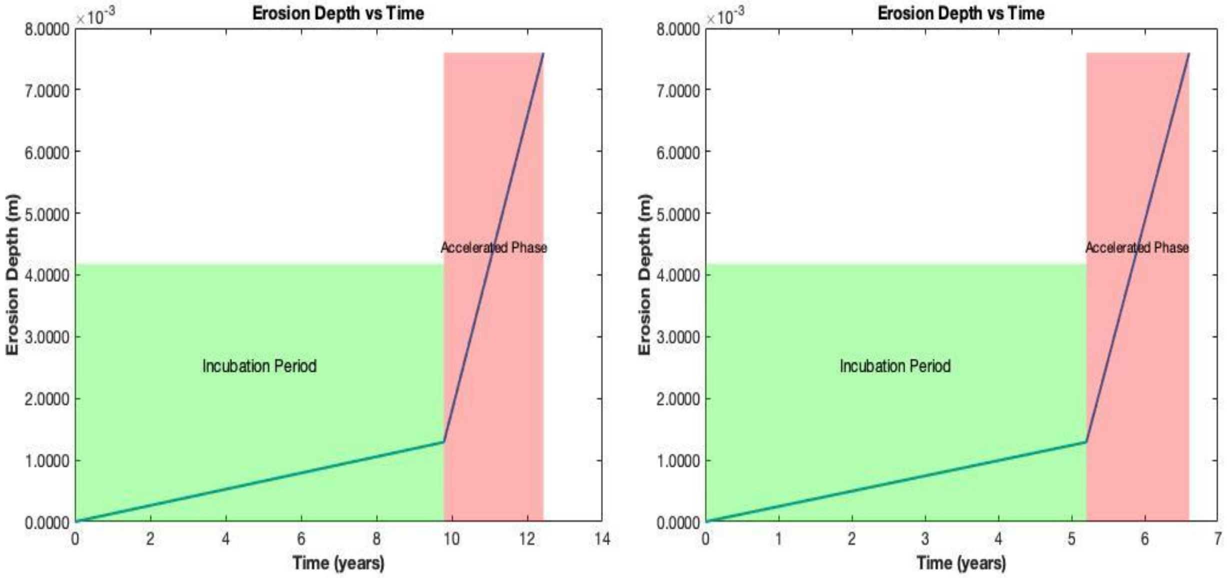

Figure 42 - Erosion Depth vs Time for Glasgow (left) and Skye (right)

The results show consistency between regions, with the trend showing a gradual increase in erosion depth during the incubation period, followed by an accelerated phase of erosion between the end of the incubation period and the failure of the material.

Considering the AEP losses from Sections 5.4.1 and 5.4.2, the results suggest that the AEP losses during the incubation period would be within the 1-5% range [15, 17, 26, 29, 50, 72] expected for these timeframes at more optimal angles of attack such as 6 and 8 degrees. With the higher angles of attack, the losses can be expected to be more extreme [16] and aligning closer to the higher end of the range of values shown in the literature [9, 17].

5.5.2 Comparison between regions

Comparing regions with varying rainfall intensities and number of yearly rainfall hours revealed significant changes in the lifetime of the coating material. Regions with higher rainfall and greater number of rainfall hours, such as Skye and Glasgow, experienced shorter incubation periods and coating lifetimes, leading to faster progression between the erosion stages and material failure. On the other hand, regions with lower rainfall intensities and annual hours of rainfall showed longer incubation periods, resulting in the delayed onset of the latter erosion stages. Furthermore, the westernmost regions were subject to the shortest coating lifetimes when compared to the northern and central regions. This validates the previous work within the field of literature, as it suggests that there are areas in which wind farm projects would be more susceptible to leading edge erosion [52].

5.5.3 Implications for wind farm projects

The observed erosion behaviour has significant implications for wind farm projects. Turbines operating in regions with longer incubation periods can expect a lower energy loss throughout their initial 15 years of operation, whereas areas with higher rainfall may begin to experience an accelerated loss of power as early as their 5th year, followed by a premature requirement for blade replacement as early as their 6th year. This can have serious financial implications for the economic viability of projects within these regions and therefore must require significant consideration during the planning stage of projects within these regions.

5.5.4 Sensitivity to Droplet Diameter

As the above analysis only varied rainfall intensity and number of hours of rainfall in estimating the time for the onset of erosion, the droplet diameter was kept constant at 1mm. In practice, this would not be the case as the droplet diameter would vary dependent of the rainfall intensity. Therefore, a sensitivity analysis was conducted to investigate the models' response to a changing droplet diameter.

The model showed significant variance in the predicted lifetime of the coating in response to change in the droplet diameter. This can be attributed to the fact that the droplet diameter is used to calculate the number of drops within a cubic metre of air, sharing a relationship of indirect proportionality between increasing drop diameter and the number of droplets with a cubic metre of air. Furthermore, the droplet diameter is used to calculate the terminal velocity of the droplets, which is also a factor within the calculation of the number of droplets. The relationship between droplet diameter, number of drops and terminal velocity can be seen in Figure 43.

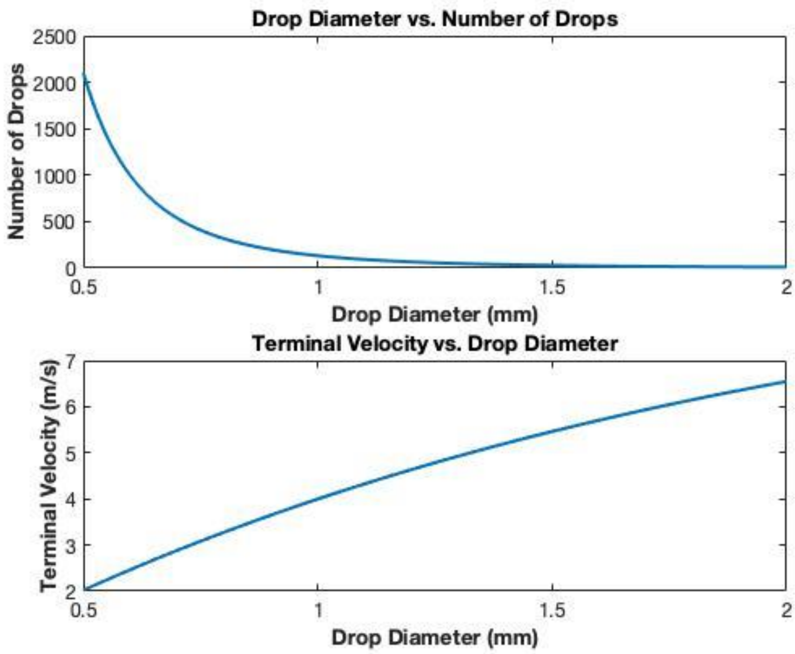

Figure 43 - Drop Diameter vs Number of Drops and Terminal Velocity

To investigate the sensitivity of the predicted lifetime output to the droplet diameter, the model was run for a 1mm diameter and constant rainfall of 1mm/hr to produce a baseline model. The droplet diameter was then raised by 1%, 5%, 10% and 15% to evaluate the change in predicted lifetime. The baseline model can be seen in Figure 44.

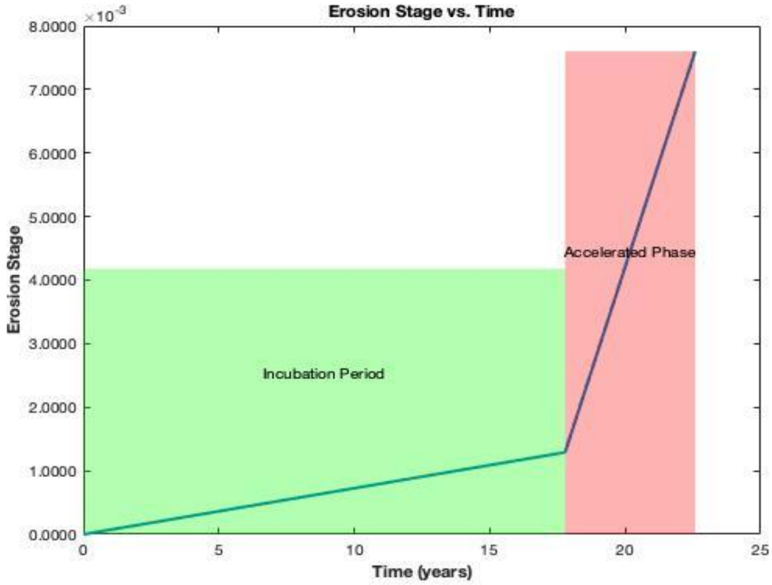

Figure 44 - Baseline Model for Sensitivity Analysis

The baseline model results showed that for a rainfall intensity of 1mm/hr and a droplet diameter of 1mm the incubation period of the coating would last 17.78 years, and total failure reached after 22.63 years. Increasing the droplet diameter by 1%, 5%, 10% and 15% showed a significant increase in lifetime for each increased diameter. The calculated lifetimes and incubation periods for the altered droplet diameters can be seen in Figure 30.

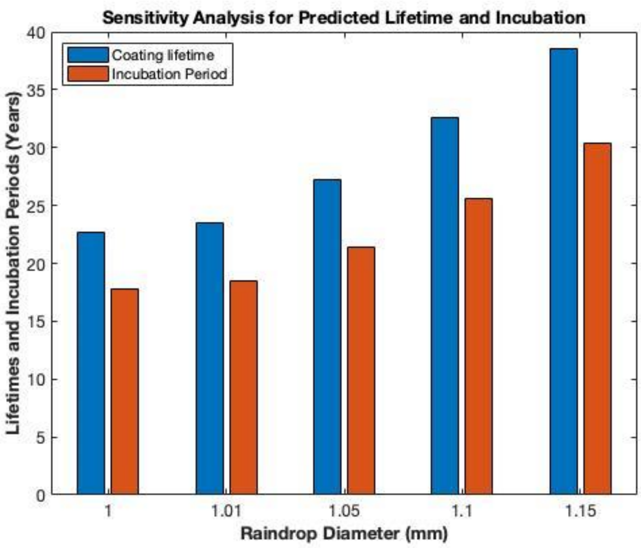

Figure 45 - Droplet Diameter Sensitivity Analysis

The results of Figure 38 show that the model is sensitive to the droplet diameter. The relationship shows that lifetime increases with droplet diameter. Figure 45 showed that the coating lifetime increased at around four times the increase in droplet diameter. The 1% increase in droplet diameter showed a 4% increase in lifetime of the coating material matched with a similar increase for the 15% increase in droplet diameter which resulted in a 70% increase in the lifetime of the coating material. This can be attributed to the relationship between droplet diameter and number of drops per cubic metre of air as with increasing droplet diameter there are less available raindrops to impact the surface. This is recognised as a limitation to the prediction of the lifetime of the coating materials as in practice, the terminal velocity, number, and diameter of drops will vary considerably throughout the operating lifespan of a turbine.

5.5.5 Erosion progression validation

These trends align with the literature, showing the increased rate of mass removal beyond the end of the incubation period or stage 3 erosion. However, the expected result has a lower gradient for both the incubation and accelerated phase. This is due to the two plots having a slightly different Y-axis, with the erosion model developed within this study showing the equivalent sand grain roughness on the Y-axis to denote the progression between erosion stages whereas the typical mass plot has mass loss on the Y-axis. The comparison between the plots is shown in Figure 46.

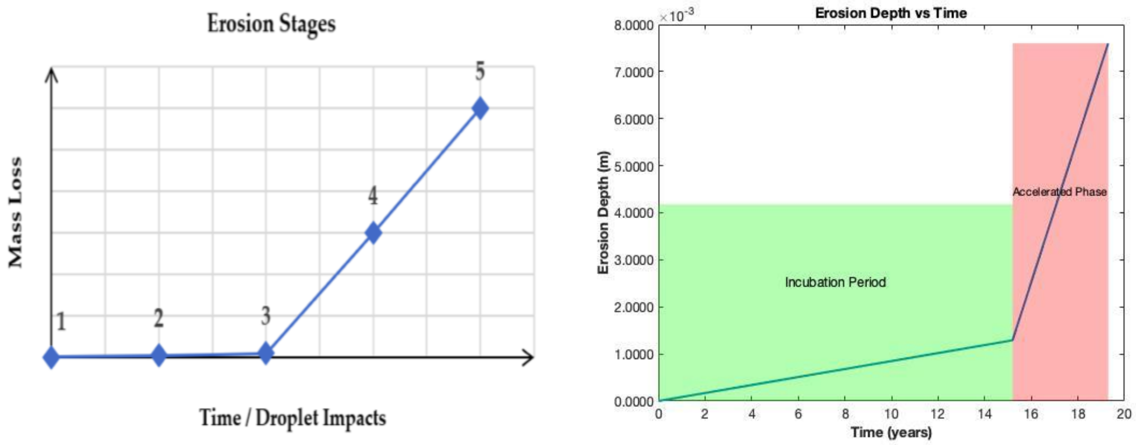

Figure 46 - Expected Erosion development trend vs Observed Erosion Development Trend

As the erosion model developed within this paper makes use of the staged approach using impact energy developed by Nash, it is important to validate the results against the findings of the staged impact energy approach. The comparison between the two plots can be seen in Figure 47.

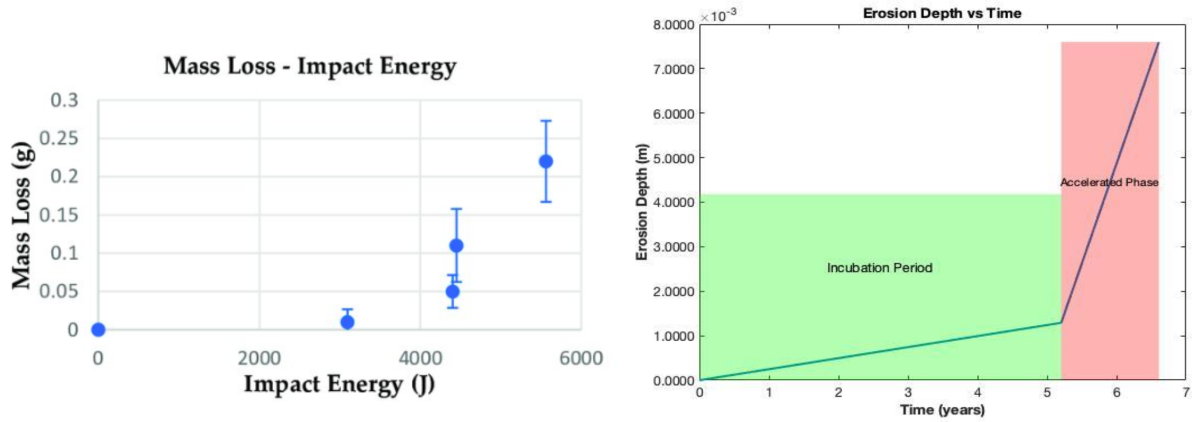

Figure 47 - Staged Approach vs Erosion Model

Upon comparison to the impact energy staged approach, it can be said that the results follow a similar trend of increasing mass loss and consequent erosion with increasing impact energy. However, the results also show that the erosion development is far more linear than the impact energy approach. This can be attributed to the differences in calculation, as the impact energy findings were the result of the use of a rain erosion testing rig whereas the erosion model only uses the relative change in impact energy between stage 3 and 5 to estimate the behaviour of the erosion during the accelerated phase.

5.6 Financial Implications

The loss in annual energy production due to leading edge erosion can have serious financial implications on the economic viability of both offshore and onshore wind projects. This impact can be quantified using the results of the lifetime of the coating materials and the annual energy production losses for each stage. Using this with the Renewable Energy Planning Database, the financial impact of leading-edge erosion on the wind sector could be estimated. A table of the parameters used for the financial analysis can be seen in Table 10.

Table 10- Financial Parameters

Parameter	Value
Onshore Capacity (GWh)	14.24 [91]

Offshore Capacity (GWh)	13.24 [91]
Onshore Capacity Factor	30% [53]
Offshore Capacity Factor	42% [53]
Assumed Energy Price (£/MWh)	47 [53]
AEP loss after 5	1.65
AEP loss after 10	3.3
AEP loss after 15	3.7
AEP loss after 20	6.2

The losses in AEP for the chosen time periods in Table 14 were calculated by interpolating between the times for the onset of each erosion stage from the coating lifetime model and using the predicted AEP losses for each stage calculated in Section 5.4. This allowed for the estimation of the losses for each year of the operating lifespan. The results of this analysis can be seen in Figure 48.

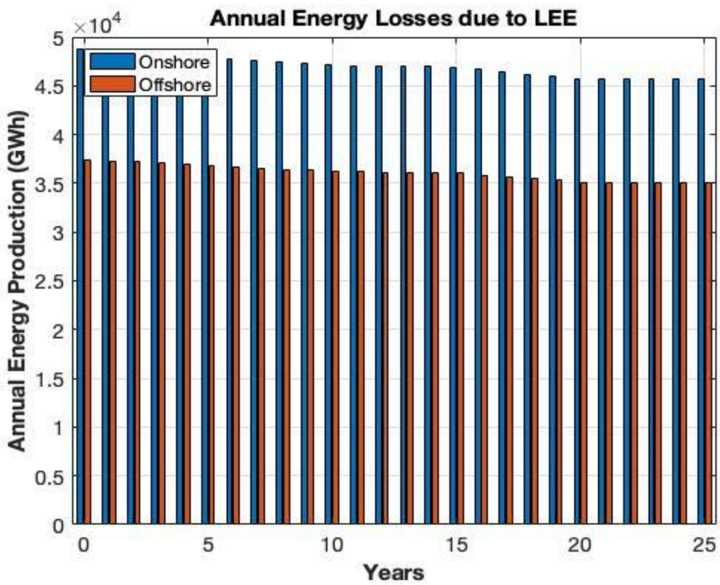

Figure 48 - Onshore and Offshore Annual Energy Losses

The results show that the AEP steadily reduces throughout the operating lifespan, before plateauing at a loss of 6.2% after the onset of stage 4 erosion. This is congruent with the literature which propose that AEP loss should fall within 1-5% for stage 4 erosion. However, these results do not fully agree with the literature in terms of the length of time for the erosion to develop. This is mainly due to variance between analytical methods, from numerical to experimental, producing different timeframes for the onset of more severe stages of erosion. The results both agree and disagree with Sareen , as the AEP loss is within the 1-25% [9] range of expected AEP loss due to the different erosion stages. The results of this paper suggest that the onset of the more severe stages of erosion take longer to develop. However, there is a lack of information for timeframes above 15 years of operation so the results of this analysis cannot be validated for a period greater than this. The results do agree with the maintenance data from the wind farm Horns Rev 2 [92] which reported severe erosion after 6 years, as the computed lifetime for Skye's rainfall characteristics was roughly 6 years with an incubation period lasting just over 5 years.

As previously mentioned, these AEP losses have great impacts on the profitability of both onshore and offshore wind projects. The yearly losses show that for the onshore wind sector, LEE could cause a yearly loss of between £5.5 and £109 million dependent on the severity of erosion. The offshore wind sector could see an average loss of between £7.5 million and £141 million per year of operation, dependent on the severity of the erosion. The financial losses per year for both sectors can be seen in Figure 49.

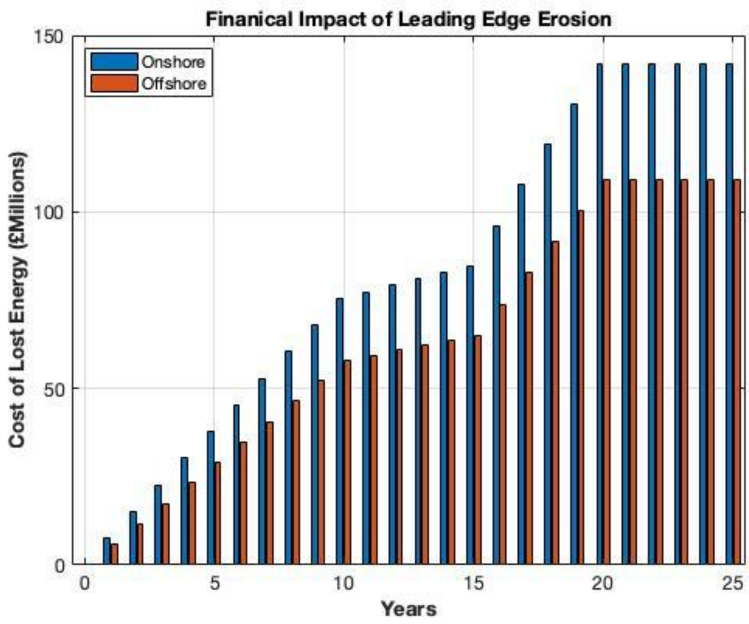

Figure 49 - Cost of Lost Energy due to LEE

Figure 34 visualises the costs associated with the increased rate of erosion between years 15 and 20 as this signals the end of the incubation period and increased material removal from the surface of the turbine blades and hence, the cost of lost energy significantly increases. Totalling the losses throughout the entirety of their operating lifespan, leading edge erosion results in a

£1.76 billion and £2.29 billion total revenue loss for the onshore and offshore wind sectors respectively. Therefore, the total lost revenue for the UK wind sector was calculated to be just over £4 billion. Upon comparison to the literature, it can be said that the results are greater than estimations from similar studies. H. Law [53] concluded that in 2019 the financial impact of LEE was £76 million under the assumption that the AEP losses would be within a range of 1-5% [53], versus the 0-6.2% used within this study. The results of H. Law fall considerably short of the estimated average yearly loss for both sectors within this study, at £161.9 million, however, this can be attributed to the increase in the UK installed capacity between 2019 [93] and 2023 [91] along with the difference in assumed AEP losses between the studies.

5.6.1 Impact of LEE on Net Present Value

The economic impact of leading-edge erosion on offshore wind farm projects, using operational data form the existing offshore wind farm Hornsea 2 off the coast of Yorkshire, was quantified and analysed. The Net Present Value (NPV) analysis was used to assess the economic viability of the project under both uneroded and eroded blade conditions, considering the parameters outlined in Table 11.

Table 11 NPV Parameters

Parameter	Value
Capacity (MW)	1386
Capital Expenditure (£)	£3,824,000,000
Operational Expenditure (£/kWh)	0.018 [94]
Current Energy Strike Price (£/MWh)	83.94 [95]
Discount Rate (%)	6% [96]
Lifespan (Years)	25

From the data in Table 16 and accounting for the AEP losses calculated in the section prior, the NPV of Hornsea 2 accounting for leading edge erosion losses was calculated to be £395.76 million. In contrast, the NPV of Hornsea 2 with the omission of the leading-edge erosion losses, was calculated to be £535.02 million. This difference indicates that leading edge erosion has directly reduced the NPV of the project by nearly £140 million.

5.7 Implications on Operations and Maintenance

As the severity of the erosion upon the blade surface progresses, operators must develop adequate repair and replacement strategies.

There are several prevention, repair and replacement strategies currently used in industry to protect the energy production of wind turbines in operation. As a preventative measure, wind turbines are being coating with increasingly durable coating materials to delay the development of erosion. Of these materials, polyurethane elastomers and epoxies have emerged as leading solutions [74, 97].

If a blade must be repaired, this can increase losses due to the downtime required for the repair. Repairs to the blades are often made through the reapplication of coating materials using fillers or the application protective tapes [78]. These tapes also affect the aerodynamic performance of the blade, but the effect is significantly lower than the losses observed during the presence of erosion [98].

Another solution which has emerged as a method of reducing the rate of erosion on the blades of wind turbines is reducing the tip-speed during periods of higher rainfall [49]. This allows for lower impact velocities upon the blade surface and hence delays the progression of erosion [78]. However, reducing the tip speed also reduces the energy production of the turbines.

5.8 Environmental Impact of LEE

This section aims to investigate the environmental impact of wind turbine leading edge erosion on its surrounding area. This section will be broken down into three subsections regarding the main environmental impacts of leading-edge erosion: Bisphenol A emissions and increased noise pollution.

5.8.1 Epoxy Resin and Bisphenol A (BPA) Considerations

Epoxy resin is commonly used in turbine blades for its excellent mechanical properties, but it contains a significant proportion of Bisphenol A (BPA), ranging between 45% and 61% dependent on the manufacturing method [99]. As these blades erode, the BPA within the epoxy is released into the environment. Solberg [100] estimates that an industry standard 136m diameter turbine emits 62kg of BPA and microplastics annually. Extrapolating this to a 20-turbine farm results in over 1.2 tonnes of BPA being emitted to the surrounding area each year and approximately 30 tonnes over a 25-year operating lifespan [51, 100].

The emission of BPA raises significant environmental concerns as it can contaminate soil, bodies of water, and air, posing threats to terrestrial and aquatic ecosystems. Offshore wind farms, chosen for optimal wind exposure, present a particular risk as they can directly release BPA into marine environments, threatening coastal ecosystems and marine life [101, 102]. The World Health Organization's estimation that 1kg of BPA can contaminate nearly 10 billion litres of water, highlighting the potential severity of releasing 1.2 tonnes of BPA per year into coastal waters [100, 103]. However, it is reported by Epoxy Europe that the annual release of BPA through the use epoxy within blades is around 92kg, significantly lower than the estimates of other studies [99, 100]. The BPA emissions data extracted from the Epoxy Europe report can be seen in Table 12.

Table 12 - BPA emissions from use of epoxy [99]

Wind rotor blades					
Total epoxy usage mass	**Total BPA releases into environment**				
	Production	**Application**	**Service life**	**Waste**	**Total**
249,365 t	948 kg	not determinable	negligible	not determinable	> 948 kg

Annual epoxy usage mass (2013)	**Annual BPA releases into environment**				
	Production	**Application**	**Service life**	**Waste**	**Total**
24,162 t	92 kg	not determinable	negligible	not determinable	> 92 kg

BPA is an endocrine disruptor, which can negatively impact reproductive health if ingested [104, 105]. Although the concentration of BPA typically found in human blood due to ingestion is not enough to cause illness, it can be particularly harmful to aquatic life, especially invertebrates and small land-based invertebrates like field mice [104, 106]. The USEPA has identified BPA as having high chronic aquatic toxicity, significantly affecting certain groups of aquatic invertebrates, molluscs, and copepods [101]. Several studies have further confirmed the major impacts of BPA on aquatic life in both freshwater and saltwater environments [101, 102, 107]. As wind energy continues to expand, addressing the release of BPA from turbine blades becomes paramount. Exploring alternative materials for blade construction and strategically selecting turbine sites away from particularly sensitive environments can help mitigate these environmental risks. It is essential for the industry to adopt measures that safeguard ecosystems and wildlife while promoting the benefits of renewable energy.

5.8.2 Noise Pollution

Another impact on the surrounding environment of wind turbines, in both eroded and uneroded conditions, is noise pollution. There are two main categories of noise produced by wind turbines: mechanical and aerodynamic.

5.8.2.1 Mechanical noise

Mechanical noise is mainly produced by the components from within the wind turbine, such as the gearbox and the generator. This noise is transmitted from the components to the surrounding area through vibrations between the components and the structural components such as the casings, nacelle covers, and the rotor blades themselves [108, 109]. Airborne noise can also be transmitted directly from the components to the surrounding area. However, mechanical noise is mitigated with relative ease in industry today through the implementation of sound insulation and vibration dampening within the nacelle [109].

5.8.2.2 Aerodynamic noise

Aerodynamic noise is a more complex issue to resolve and is the more prominent source of noise that is emitted from wind turbines. The aerodynamic noise varies with the operating conditions of the turbine and can vary for different regions of the turbine blade. These regions create their own specific noises with different characteristics and do not interfere with each other due to their placement along the blade geometry. The main noise classifications are turbulent boundary layer noise, laminar boundary layer vortex shedding noise, separation stall noise, trailing edge bluntness vortex shedding noise, tip vortex formation noise and noise due to turbulent inflow [110]. Figure 50 visualises these noise sources for a given rotor blade with wind velocity, U.

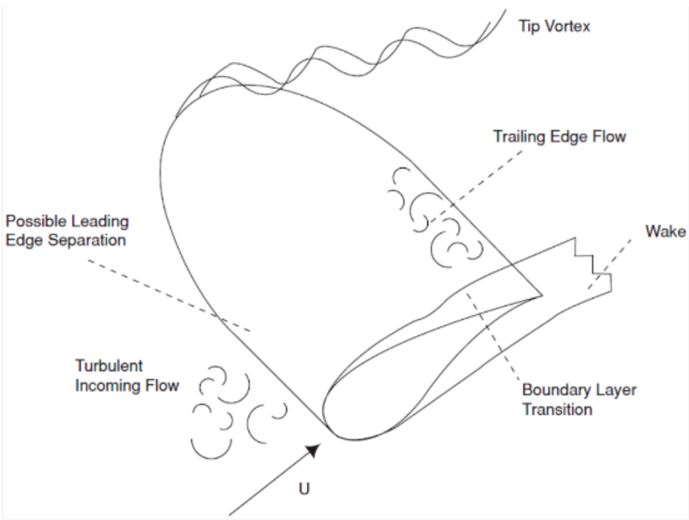

Figure 50 - Aerodynamic Noise Sources [111]

As these noises are generated by aerodynamic effects of the wind flow over the rotor blade, leading edge erosion can have a significant impact on the magnitude of the noise that is generated. Wang [112] concluded that leading edge erosion has a notable impact on the aerodynamic noise created by wind turbines, with a particular increase around the 50-200Hz and 400-100Hz ranges. The study concluded that the overall sound pressure level (OASPL) for light erosion, spanning 1% of the chord length at a depth of 0.5mm, increased by 5.4dB. Furthermore, for severe erosion stages, spanning 10% of the chord length at a depth of 1mm, the OASPL increased by 8dB [111].

5.8.2.3 Environmental Impact of Noise Pollution

Wind turbine noise has implications on the behaviour of the surrounding wildlife and ecosystem. There have been many studies into the impacts of anthropogenic noise [111, 113] on wildlife, all of which agree that noise pollution can disrupt crucial survival mechanisms. A study into noise pollution by Teff-Seker [111] highlights that there are four main potential impacts from anthropogenic noise on surrounding wildlife. Firstly, the noise can cause physiological damage by increasing the level of stress hormones to dangerous levels, or worse, cause hearing loss which can impact the ability of certain species to detect threats or locate prey. Moreover, the noise can be directly perceived by animals as a threat causing them to behave in an anti-predatory manner at the expense of their usual foraging behaviours [114], this is often seen in species of squirrel local to the regions of wind turbines. Furthermore, species which do continue their typical foraging behaviours often see reduced efficiency in finding and handling food. In more severe cases, the threat can be perceived to be so great that species may leave the affected area altogether [115] which contributes to a functional habitat loss around the area of the wind turbine installation. Finally, species which rely on signal frequencies to detect threats and prey, will suffer from a reduced range in which a signal can be detected along with the amount of information which can be interpreted from this signal [113, 116], such as the sound of an approaching predator. Therefore, it can be said that noise pollution has an impact on animal communities, reduces their ability to respond to threats and opportunities which ultimately jeopardises their overall survival, hence contributing to the decline in biodiversity in regions with wind farm developments.

With the above impacts of existing wind turbine noise highlighted, it becomes apparent that the impact of increased aerodynamic noise because of leading-edge erosion will have an even greater detrimental effect on the wildlife in these areas. As Wang highlighted, there are specific ranges in which leading edge erosion will contribute to an increased OASPL, suggesting that not all wildlife will experience an increased disruption to their usual behaviours due to increased noise. However, some of species' which operate within the 400-1000Hz range that is particularly impacted by LEE, are birds, rodents, crustaceans, and bats [117, 118] which are common to the local regions of offshore and onshore wind farm developments. This highlights that the most likely species to be impacted by an increased aerodynamic noise are the species most local to these developments. However, within the planning stages of wind turbine developments, significant EIA analysis is undertaken to ensure that the impact of noise pollution is minimised and in best case, mitigated entirely through careful site selection and restoration measures.

6.0 Conclusions

This paper has proposed a framework for analysing the impact of LEE on both the aerodynamic and operational performance using computational fluid dynamics approach to investigate the aerodynamic effect of LEE and extrapolating this effect to estimate the impact on operational performance. Furthermore, the proposed framework also considers the temporal development of LEE, estimating the periods of operation in which the turbine will experience gradual and accelerated energy loss.

The analysis concluded that there is a significant aerodynamic impact on wind turbine blades as a result of leading-edge erosion, with the coefficient of lift decreasing by as much as 35% paired with a potential 153.15% increase in the C_d for more severe erosion stages. The simulations showed that LEE is has a more significant impact at higher angles of attack, furthermore, LEE was shown to lower the optimal AoA for lift-to-drag generation, from 8 degrees to 6, for the chosen aerofoil. The estimated power coefficients for the eroded blades showed that with increasing LEE stage, the lower the maximum achievable power coefficient. The Power Coefficients ranged from 0.388 to 0.496, which is largely congruent with the operating power coefficients of turbines today which are within the range of 0.4-0.5. The power curves produced for the given input parameters showed that the power capacity was also influenced by leading edge erosion, with reductions ranging from 4.7% to 20% for the most severe stage of erosion. Estimating the AEP losses as a result of the reduced power coefficients and power curves showed that losses due to LEE can range from 1.65% to 18.4% dependent on the stage of erosion and the AoA. These results fall within the range of values from previous studies for the AEP losses for a wind turbine due to LEE, highlighting the validity of the proposed framework and methodology.

The sector-wide financial implications of LEE were estimated using the Renewable Energy Planning Database to identify the current installed capacity within the UK. The financial loss over the operating lifetime of a wind turbine was estimated to be £4 billion, with an average yearly loss of £161.9 million. This disagrees with previous studies into these financial implications which estimated a sector-wide loss of £76 million with the assumption that losses ranged from 1-5% [37], however, the losses and installed capacity used within this study were greater. Furthermore, using Hornsea 2 as a case study, the NPV was calculated for both eroded and uneroded blades to estimate the impact of LEE on the economic viability of wind farm projects. The NPV reduction due to LEE was estimated to be £140 million for Hornsea 2, highlighting the significance of LEE to wind farm projects.

The erosion rate and coating lifetime model showed that for four different regions, the predicted lifetime of the blades was significantly different, ranging from 6 years to over 19 years. The erosion model was recognised to be highly sensitive to the meteorological inputs, especially the droplet diameter. A sensitivity analysis was conducted and showed that the lifetime was changing at approximately 4x the rate of change of droplet diameter. However, the results of the temporal progression of erosion disagreed with the Staged Approach by Nash, with the results of this study showing a more linear erosion development than the results of Nash. However, the graphs were not directly comparable which may have been the cause for the disparity between the two graphs.

Evaluation and validation of the results showed that the model successfully estimated the impact of LEE on the aerodynamic and operational performance using surface roughness. However, the model displayed a slight overestimation in lift and drag values when compared to published values for the NACA4412. Despite this, the percentage increase in drag was found to be within the range of the published values. The peak values estimated within this study were higher than some of the published values for AEP loss, but this was attributed to the use of the stall angle within this analysis which showed an overestimation in drag compared to the other angles. Overall, the proposed framework can estimate the impact of LEE on wind turbine blades using surface roughness and estimate the temporal development of this erosion throughout a wide range of stages, suggesting that it could prove to be a useful tool within this research area.

7.0 Future Work

The analysis of the aerodynamic impact of LEE, the temporal development of the different erosion stages for different climates, and the overall performance loss highlighted that the framework presented within this study can be used to analyse the aerodynamic and performance losses of wind turbine blades due to leading edge erosion. Furthermore, the framework can be used for varying regions to estimate the temporal development of leading-edge erosion to predict the time at which significant energy production loss should be expected. However, the framework could be further applied to consider the impact of different particle impacts, such as solid particles like sand and hail. A further extension of this, could also allow for the consideration of multiple different particle impacts at once as opposed to analysing their impact in isolation.

One of the limitations of the framework, is that it assumes a constant droplet diameter and constant impact velocity for the rain droplet impacts. An improvement could be made to include the variation of impact velocities and droplet diameters to estimate the rate of erosion and its potential impacts more accurately. This could be achieved by integrating the probabilistic raindrop diameter function for different rain rates and to further develop the relationship between erosion and the meteorological parameters. This would allow the framework to sufficiently vary the meteorological parameters such as droplet terminal velocity and the number of drops per cubic metre of air to create more accurate estimations of the impacts on the blades.

Finally, as the erosion is considered uniform along the blade profile, one more improvement that could be made to the framework is to develop a method for varying the erosion along the blade profile which would more accurately reflect the behaviour of LEE in practice. This could also be extended to a 3D model with multiple blade profile sections to emulate a real-life scenario more closely. This would serve as a valuable analytical tool for wind turbine developers and could form a useful future research project.

8.0 References

[1] M. Elhadi Ibrahim and M. Medraj, "Water Droplet Erosion of Wind Turbine Blades: Mechanics, Testing, Modeling and Future Perspectives," *Materials*, vol. 13, no. 1, doi: 10.3390/ma13010157.

[2] D. Eisenberg, S. Laustsen, and J. Stege, "Wind turbine blade coating leading edge rain erosion model: Development and validation," *Wind Energy*, https://doi.org/10.1002/we.2200 vol. 21, no. 10, pp. 942-951, 2018/10/01 2018, doi: https://doi.org/10.1002/we.2200.

[3] IEA. "Wind Technology and Deployment." IEA. (accessed.

[4] MetOffice. "Climate Summaries." Met Office. (accessed 13/03/23, 2023).

[5] J. L. Tangler and D. M. Somers, "NREL Airfoil Families for HAWTs," National Renewable Energy Laboratory, 1995.

[6] M. Molina and P. Mercado, "Modelling and Control Design of Pitch-Controlled Variable Speed Wind Turbines," 2011.

[7] M. Chakraborty, "A Computational Study on two horizontally close sequential airfoils to determine conjoined pressure distribution and aerodynamic influences on each other," 2015.

[8] G. Gupta, D. Kaushik, Kushagramathur, R. Pal, and P. Bhatnagar, "Power Generation through Wind Turbine in Locomotives & validation of performance parameters for a Bi-Directional Wind Turbine: Wells Turbine," *International Journal of Engineering Technology, Management and Applied Sciences*, vol. 4, 05/01 2016.

[9] A. Sareen, C. A. Sapre, and M. S. Selig, "Effects of leading edge erosion on wind turbine blade performance," *Wind Energy*, https://doi.org/10.1002/we.1649 vol. 17, no. 10, pp. 1531-1542, 2014/10/01 2014, doi: https://doi.org/10.1002/we.1649.

[10] "Britain produced record amount of wind power in 2022," Reuters, 2023.

[11] renewableUK. "Wind Energy Statistics." renewableUK. (accessed 5th March, 2023).

[12] T. D. f. E. S. a. N. Zero, "Offshore Wind Net Zero Investment Roadmap," HM Government, 2023.

[13] R. Norris, "Government’s planning reforms fail to bring back onshore wind in England," ed: renewableUK, 2023.

[14] E. Cortés, F. Sánchez, A. O’Carroll, B. Madramany, M. Hardiman, and T. M. Young, "On the Material Characterisation of Wind Turbine Blade Coatings: The Effect of Interphase Coating–Laminate Adhesion on Rain Erosion Performance," *Materials*,

vol. 10, no. 10, p. 1146, 2017. [Online]. Available: https://www.mdpi.com/1996-1944/10/10/1146.

[15] K. Panthi and G. V. Iungo, "Quantification of wind turbine energy loss due to leading-edge erosion through infrared-camera imaging, numerical simulations, and assessment against SCADA and meteorological data," *Wind Energy,* https://doi.org/10.1002/we.2798 vol. 26, no. 3, pp. 266-282, 2023/03/01 2023, doi: https://doi.org/10.1002/we.2798.

[16] W. Han, J. Kim, and B. Kim, "Effects of contamination and erosion at the leading edge of blade tip airfoils on the annual energy production of wind turbines," *Renewable Energy,* vol. 115, pp. 817-823, 2018/01/01/ 2018, doi: https://doi.org/10.1016/j.renene.2017.09.002.

[17] Y. Wang, L. Wang, C. Duan, J. Zheng, Z. Liu, and G. Ma, "CFD simulation on wind turbine blades with leading edge erosion," *Journal of Theoretical and Applied Mechanics,* journal article vol. 59, no. 4, pp. 579-593, 2021, doi: 10.15632/jtam-pl/141546.

[18] S. Emani, S. Vandrangi, and G. Velidi, *Various Approaches to Increase the Aerodynamic Efficiency for Airfoils at Low Reynolds Number Flows*. 2012.

[19] R. Gao and Z. Gao, "Pitch control for wind turbine systems using optimization, estimation and compensation," *Renewable Energy,* vol. 91, pp. 501-515, 2016/06/01/ 2016, doi: https://doi.org/10.1016/j.renene.2016.01.057.

[20] M. Nabhan, "Study of Theoretical and Numerical Fluid Characteristics of Plain Wing with Winglets," *IOP Conference Series: Materials Science and Engineering,* vol. 370, p. 012027, 05/01 2018, doi: 10.1088/1757-899X/370/1/012027.

[21] DynamicFlight. "Drag." DynamicFlight. http://www.dynamicflight.com/aerodynamics/drag/#:~:text=Profile%20Drag%20is%20the%20drag,result%20of%20production%20of%20lift. (accessed 13th June, 2023).

[22] T. S. "Understanding Parasite and Induced Drag." Medium. https://medium.com/how-to-aviation/understanding-parasite-and-induced-drag-e629dd97997e (accessed.

[23] T. Benson. "The Drag Coefficient." NASA. https://www.grc.nasa.gov/www/k-12/VirtualAero/BottleRocket/airplane/dragco.html (accessed.

[24] AirShaper. "What is a Drag Coefficient?" AirShaper. https://airshaper.com/videos/what-is-a-drag-coefficient/bEgoZ_dAg7o (accessed 13th June, 2023).

[25] L. Mishnaevsky *et al.*, "Leading edge erosion of wind turbine blades: Understanding, prevention and protection," *Renewable Energy*, vol. 169, pp. 953-969, 2021/05/01/ 2021, doi: https://doi.org/10.1016/j.renene.2021.01.044.

[26] M. S. Campobasso, A. Castorrini, L. Cappugi, and A. Bonfiglioli, "Experimentally validated three-dimensional computational aerodynamics of wind turbine blade sections featuring leading edge erosion cavities," *Wind Energy*, https://doi.org/10.1002/we.2666 vol. 25, no. 1, pp. 168-189, 2022/01/01 2022, doi: https://doi.org/10.1002/we.2666.

[27] R. S. Ehrmann, B. Wilcox, E. B. White, and D. C. Maniaci, "Effect of Surface Roughness on Wind Turbine Performance," United States, 2017. [Online]. Available: https://www.osti.gov/biblio/1596202

https://www.osti.gov/servlets/purl/1596202

[28] D. C. Maniaci, "Leading Edge Erosion Measurement and Modeling Campaigns," Sandia National Lab.(SNL-NM), Albuquerque, NM (United States), 2016.

[29] I. F. Zidane, K. M. Saqr, G. Swadener, X. Ma, and M. F. Shehadeh, "On the role of surface roughness in the aerodynamic performance and energy conversion of horizontal wind turbine blades: a review," *International Journal of Energy Research*, https://doi.org/10.1002/er.3580 vol. 40, no. 15, pp. 2054-2077, 2016/12/01 2016, doi: https://doi.org/10.1002/er.3580.

[30] D. Li, R. Li, C. Yang, and X. Wang, "Effects of Surface Roughness on Aerodynamic Performance of a Wind Turbine Airfoil," in *2010 Asia-Pacific Power and Energy Engineering Conference*, 28-31 March 2010 2010, pp. 1-4, doi: 10.1109/APPEEC.2010.5448702.

[31] G. R. Fischer, T. Kipouros, and A. M. Savill, "Multi-objective optimisation of horizontal axis wind turbine structure and energy production using aerofoil and blade properties as design variables," *Renewable Energy*, vol. 62, pp. 506-515, 2014/02/01/ 2014, doi: https://doi.org/10.1016/j.renene.2013.08.009.

[32] M. R. Islam, L. B. Bashar, D. K. Saha, and N. S. Rafi, "Comparison and Selection of Airfoils for Small Wind Turbine between NACA and NREL's S series Airfoil Families," *International Journal of Research in Electrical, Electronics and Communication Engineering*, vol. 4, no. 2, pp. 1-11, 2019.

[33] R. Febriyanto *et al.*, "Study experimental of blade NACA 4412 with pitch angle on horizontal wind turbine," *Journal of Physics: Conference Series,* vol. 1153, no. 1, p. 012137, 2019/02/01 2019, doi: 10.1088/1742-6596/1153/1/012137.

[34] M. Kevadiya and H. Vaidya, "2D ANALYSIS OF NACA 4412 AIRFOIL," *International Journal of Innovative Research in Science, Engineering and Technology,* vol. 02, pp. 1686-1691, 05/01 2013.

[35] C. J. V. Upadhyay Harsh Klritbhai, "2D ANALYSIS OF NACA 4412 SERIES WIND BLADE AT DIFFERENT ANGLE OF ATTACK," *International Research Jounral of Engineering and Technology,* vol. 7, no. 6, 2020.

[36] S. E. Mouhsine, K. Oukassou, M. M. Ichenial, B. Kharbouch, and A. Hajraoui, "Aerodynamics and structural analysis of wind turbine blade," *Procedia Manufacturing,* vol. 22, pp. 747-756, 2018/01/01/ 2018, doi: https://doi.org/10.1016/j.promfg.2018.03.107.

[37] U. Mamadaminov, "Review of Airfoil Structure for Wind Turbine Blades," 09/12 2013.

[38] K. Mulder, *Sustainability Made in Delft*. 2006.

[39] W. Timmer and R. P. J. O. M. Rooij, "Summary of the Delft University Wind Turbine Dedicated Airfoils," *Journal of Solar Energy Engineering-transactions of The Asme - J SOL ENERGY ENG,* vol. 125, 01/06 2003, doi: 10.1115/1.1626129.

[40] D. V. T. David Heffley, "Aerodynamic Characteristics of the NACA4412 Aerofoil," Baylor University, 2007.

[41] M. Petinrin and V. Onoja, "Computational Study of Aerodynamic Flow over NACA 4412 Airfoil," *British Journal of Applied Science & Technology,* vol. 21, pp. 1-11, 01/10 2017, doi: 10.9734/BJAST/2017/31893.

[42] S. Kale and R. Varma, "Aerodynamic Design of a Horizontal Axis Micro Wind Turbine Blade Using NACA 4412 Profile," *International Journal of Renewable Energy Research,* vol. 4, pp. 69-72, 03/28 2014, doi: 10.20508/ijrer.06222.

[43] B. Susilo, G. Jatisukamto, and M. Kustanto, "Characteristic Analysis of Horizontal Axis Wind Turbine Using Airfoil NACA 4712," *Journal of Mechanical Engineering Science and Technology,* vol. 3, pp. 96-108, 11/30 2019, doi: 10.17977/um016v3i22019p096.

[44] R. Balijepalli, U. Rajak, A. Dasore, A. Raj, and P. K. Chaurasiya, "Design and Optimization of NACA 0012, NACA 4412 and NACA 23,012 Aerofoils of Wind Turbine of Solar Updraft Tower Power Plant," in *Technology Innovation in*

Mechanical Engineering: Select Proceedings of TIME 2021, P. K. Chaurasiya, A. Singh, T. N. Verma, and U. Rajak Eds. Singapore: Springer Nature Singapore, 2022, pp. 9-18.

[45] K. Koca, M. S. Genç, H. H. Açıkel, M. Çağdaş, and T. M. Bodur, "Identification of flow phenomena over NACA 4412 wind turbine airfoil at low Reynolds numbers and role of laminar separation bubble on flow evolution," *Energy*, vol. 144, pp. 750-764, 2018/02/01/ 2018, doi: https://doi.org/10.1016/j.energy.2017.12.045.

[46] R. Herring, K. Dyer, F. Martin, and C. Ward, "The increasing importance of leading edge erosion and a review of existing protection solutions," *Renewable and Sustainable Energy Reviews*, 2019.

[47] Y. Zhang, F. Avallone, and S. Watson, "Leading edge erosion detection for a wind turbine blade using far-field aerodynamic noise," *Applied Acoustics*, vol. 207, 2023.

[48] J. Lucena, "Lamination and Delamination in Wind Turbine blades," ed: Windmills Tech.

[49] J. I. Bech, C. B. Hasager, and C. Bak, "Extending the life of wind turbine blade leading edges by reducing the tip speed during extreme precipitation events," *Wind Energ. Sci.*, vol. 3, no. 2, pp. 729-748, 2018, doi: 10.5194/wes-3-729-2018.

[50] J. C. López, A. Kolios, L. Wang, and M. Chiachio, "A wind turbine blade leading edge rain erosion computational framework," *Renewable Energy*, vol. 203, pp. 131-141, 2023/02/01/ 2023, doi: https://doi.org/10.1016/j.renene.2022.12.050.

[51] M. H. Keegan, "Wind turbine blade leading edge erosion : an investigation of rain droplet and hailstone impact induced damage mechanisms," 2014.

[52] K. Pugh and M. M. Stack, "Rain Erosion Maps for Wind Turbines Based on Geographical Locations: A Case Study in Ireland and Britain," *Journal of Bio- and Tribo-Corrosion*, vol. 7, no. 1, p. 34, 2021/01/22 2021, doi: 10.1007/s40735-021-00472-0.

[53] H. Law and V. Koutsos, "Leading edge erosion of wind turbines: Effect of solid airborne particles and rain on operational wind farms," *Wind Energy*, vol. 23, no. 10, pp. 1955-1965, 2020, doi: https://doi.org/10.1002/we.2540.

[54] Y. Zhang, F. Avallone, and S. Watson, "Leading edge erosion detection for a wind turbine blade using far-field aerodynamic noise," *Applied Acoustics*, vol. 207, p. 109365, 2023/05/01/ 2023, doi: https://doi.org/10.1016/j.apacoust.2023.109365.

[55] Y. Wang, Y. Zhou, C. Duan, L. Wang, and A. Jia, "Insight into the effects of leading edge delamination on the aerodynamic performance of an airfoil and wind turbine,"

Journal of Renewable and Sustainable Energy, vol. 14, no. 2, p. 023305, 2022, doi: 10.1063/5.0075123.

[56] D. Nash, G. Leishman, C. Mackie, K. Dyer, and L. Yang, "A Staged Approach to Erosion Analysis of Wind Turbine Blade Coatings," *Coatings*, vol. 11, p. 681, 06/05 2021, doi: 10.3390/coatings11060681.

[57] G. Duthé, I. Abdallah, S. Barber, and E. Chatzi, "Modeling and Monitoring Erosion of the Leading Edge of Wind Turbine Blades," *Energies*, vol. 14, p. 7262, 11/03 2021, doi: 10.3390/en14217262.

[58] G. S. Springer and C. I. Yang, "Model for the rain erosion of fiber reinforced composites," *AIAA journal*, vol. 13, no. 7, pp. 877-883, 1975.

[59] G. S. Springer and C. B. Baxi, "A model for rain erosion of homogeneous materials," *Erosion, Wear, and Interfaces with Corrosion*, pp. 106-124, 1974.

[60] J. J. Kauzlarich, "The Palmgren-Miner rule derived," in *Tribology Series*, vol. 14, D. Dowson, C. Taylor, M. Godet, and D. Berthe Eds.: Elsevier, 1989, pp. 175-179.

[61] N. Hoksbergen, R. Akkerman, and I. Baran, "The Springer Model for Lifetime Prediction of Wind Turbine Blade Leading Edge Protection Systems: A Review and Sensitivity Study," *Materials*, vol. 15, no. 3, doi: 10.3390/ma15031170.

[62] S. Fæster, N. F.-J. Johansen, L. Mishnaevsky Jr, Y. Kusano, J. I. Bech, and M. B. Madsen, "Rain erosion of wind turbine blades and the effect of air bubbles in the coatings," *Wind Energy*, https://doi.org/10.1002/we.2617 vol. 24, no. 10, pp. 1071-1082, 2021/10/01 2021, doi: https://doi.org/10.1002/we.2617.

[63] C. Siddons, C. Macleod, L. Yang, and M. Stack, *An experimental approach to analysing rain droplet impingement on wind turbine blade materials*. 2015.

[64] H. Slot, "A fatigue-based model for the droplet impingement erosion incubation period," PhD, Laboratory for Surface Technology and Tribology, University of Twente, 2021.

[65] H. Macdonald, D. Infield, D. H. Nash, and M. M. Stack, "Mapping hail meteorological observations for prediction of erosion in wind turbines," *Wind Energy*, https://doi.org/10.1002/we.1854 vol. 19, no. 4, pp. 777-784, 2016/04/01 2016, doi: https://doi.org/10.1002/we.1854.

[66] M. Keegan, Hugh, D. Nash, and M. Stack, *Numerical Modelling of Hailstone Impact on the Leading Edge of a Wind Turbine Blade*. 2013.

[67] N. C. Knight and A. J. Heymsfield, "Measurement and Interpretation of Hailstone Density and Terminal Velocity," (in English), *Journal of Atmospheric Sciences*, vol.

40, no. 6, pp. 1510-1516, 01 Jun. 1983 1983, doi: https://doi.org/10.1175/1520-0469(1983)040<1510:MAIOHD>2.0.CO;2.

[68] C. Dieling, M. Smith, and M. Beruvides, "Review of Impact Factors of the Velocity of Large Hailstones for Laboratory Hail Impact Testing Consideration," *Geosciences*, vol. 10, no. 12, doi: 10.3390/geosciences10120500.

[69] M. Carraro, F. De Vanna, F. Zweiri, E. Benini, A. Heidari, and H. Hadavinia, "CFD Modeling of Wind Turbine Blades with Eroded Leading Edge," *Fluids,* vol. 7, no. 9, p. 302, 2022. [Online]. Available: https://www.mdpi.com/2311-5521/7/9/302.

[70] A. Koodly Ravishankara, H. Özdemir, and E. van der Weide, "Analysis of leading edge erosion effects on turbulent flow over airfoils," *Renewable energy,* vol. 172, p. 765, 2021, doi: 10.1016/j.renene.2021.03.021.

[71] K. A. Flack, M. P. Schultz, and R. J. Volino, "The effect of a systematic change in surface roughness skewness on turbulence and drag," *International Journal of Heat and Fluid Flow,* vol. 85, p. 108669, 2020/10/01/ 2020, doi: https://doi.org/10.1016/j.ijheatfluidflow.2020.108669.

[72] K. Pugh, J. W. Nash, G. Reaburn, and M. M. Stack, "On analytical tools for assessing the raindrop erosion of wind turbine blades," *Renewable and Sustainable Energy Reviews,* vol. 137, p. 110611, 2021/03/01/ 2021, doi: https://doi.org/10.1016/j.rser.2020.110611.

[73] C. Mackie, D. Nash, D. Boyce, M. Wright, and K. Dyer, "Characterisation of a Whirling Arm Erosion Test Rig," in *2018 Asian Conference on Energy, Power and Transportation Electrification (ACEPT)*, 30 Oct.-2 Nov. 2018 2018, pp. 1-6, doi: 10.1109/ACEPT.2018.8610804.

[74] J. I. Bech, N. F.-J. Johansen, M. B. Madsen, Á. Hannesdóttir, and C. B. Hasager, "Experimental study on the effect of drop size in rain erosion test and on lifetime prediction of wind turbine blades," *Renewable Energy,* vol. 197, pp. 776-789, 2022/09/01/ 2022, doi: https://doi.org/10.1016/j.renene.2022.06.127.

[75] R. Herring *et al.*, "Assessment of a Wind Turbine Blade Erosion Lifetime Prediction Model with Industrial Protection Materials and Testing Methods," *Coatings,* vol. 11, no. 7, doi: 10.3390/coatings11070767.

[76] C. J. Spruce, "Power performance of active stall wind turbines with blade contamination," 2006.

[77] M. Ge, H. Zhang, Y. Wu, and Y. Li, "Effects of leading edge defects on aerodynamic performance of the S809 airfoil," *Energy Conversion and Management*, vol. 195, pp. 466-479, 09/01 2019, doi: 10.1016/j.enconman.2019.05.026.

[78] R. Herring, K. Dyer, F. Martin, and C. Ward, "The increasing importance of leading edge erosion and a review of existing protection solutions," *Renewable and Sustainable Energy Reviews*, vol. 115, p. 109382, 2019/11/01/ 2019, doi: https://doi.org/10.1016/j.rser.2019.109382.

[79] P. Spalart and S. Allmaras, "A one-equation turbulence model for aerodynamic flows," in *30th Aerospace Sciences Meeting and Exhibit*, (Aerospace Sciences Meetings: American Institute of Aeronautics and Astronautics, 1992.

[80] J. F. Manwell, J. G. McGowan, and A. L. Rogers, *Wind energy explained: theory, design and application*. John Wiley & Sons, 2010.

[81] A. Abo-Khalil *et al.*, "Design of State Feedback Current Controller for Fast Synchronization of DFIG in Wind Power Generation Systems," *Energies*, vol. 12, p. 2427, 06/24 2019, doi: 10.3390/en12122427.

[82] L. Domenech, J. Renau, A. Šakalytė, and F. Sánchez López, "Top Coating Anti-Erosion Performance Analysis in Wind Turbine Blades Depending on Relative Acoustic Impedance. Part 1: Modelling Approach," *Coatings*, vol. 10, p. 685, 07/16 2020, doi: 10.3390/coatings10070685.

[83] L. Domenech, V. García-Peñas, A. Šakalytė, D. Francis, E. Skoglund, and F. Sánchez López, "Top Coating Anti-Erosion Performance Analysis in Wind Turbine Blades Depending on Relative Acoustic Impedance. Part 2: Material Characterization and Rain Erosion Testing Evaluation," *Coatings*, vol. 10, p. 709, 07/22 2020, doi: 10.3390/coatings10080709.

[84] D. Atlas, R. C. Srivastava, and R. S. Sekhon, "Doppler radar characteristics of precipitation at vertical incidence," *Reviews of Geophysics*, https://doi.org/10.1029/RG011i001p00001 vol. 11, no. 1, pp. 1-35, 1973/02/01 1973, doi: https://doi.org/10.1029/RG011i001p00001.

[85] A. C. Best, "The size distribution of raindrops," *Quarterly Journal of the Royal Meteorological Society*, vol. 76, no. 327, pp. 16-36, 1950/01/01 1950, doi: https://doi.org/10.1002/qj.49707632704.

[86] N. Barfknecht, M. Kreuseler, D. De Tavernier, and D. Von Terzi, "Performance analysis of wind turbines with leading-edge erosion and erosion-safe mode operation," 2022, vol. 2265: IOP Publishing, 3 ed., p. 032009.

[87] M. Papadakis, S.-C. Wong, A. Rachman, K. E. Hung, G. T. Vu, and C. S. Bidwell, "Large and small droplet impingement data on airfoils and two simulated ice shapes," 2007.

[88] C. Rumsey. "2D NACA 4412 Airfoil Trailing Edge Separation Validation Case." NASA Langley Research Center. https://turbmodels.larc.nasa.gov/naca4412sep_val_sa.html (accessed 2023).

[89] M. Ragheb, "Optimal rotor tip speed ratio," *Lecture notes of Course no. NPRE,* vol. 475, 2014.

[90] M. A. Yurdusev, R. Ata, and N. S. Çetin, "Assessment of optimum tip speed ratio in wind turbines using artificial neural networks," *Energy,* vol. 31, no. 12, pp. 2153-2161, 2006/09/01/ 2006, doi: https://doi.org/10.1016/j.energy.2005.09.007.

[91] E. a. I. S. Department for Business. Renewable Energy Planning Database (REPD)

[92] Weston and David. "Horns Rev 2 set for blade upgrade." haymarket Media Group Ltd. (accessed.

[93] G. Goodman and V. Martin, "Wind powered electricity in the UK," United Kingdom Government, 2020.

[94] IRENA, "Renewable Energy Cost Analysis: Wind Power," IRENA, 2012, vol. 1.

[95] L. C. C. Company. Hornsea 2 (Phase I)

[96] O. Catapult. "Wind Farm Costs." ORE Catapult. (accessed 28th June, 2023).

[97] C. Hasager, L. Mishnaevsky Jr, C. Bak, J. I. Bech, S. Fæster, and N. F.-J. Johansen, "How can we combat leading-edge erosion on wind turbine blades?," *Danmarks Tekniske Universitet, Institut for Vindenergi, Risø Campus,* vol. 4000, 2021.

[98] A. Sareen, C. Sapre, and M. Selig, "Effects of Leading-Edge Protection Tape on Wind Turbine Blade Performance," *Wind Engineering,* vol. 36, pp. 525-534, 10/01 2012, doi: 10.1260/0309-524X.36.5.525.

[99] E. Europe, "Epoxy Resins in Wind Energy Applications," 2015.

[100] A. Solberg, B.-E. Rimereit, and J. Weinbach, "Leading Edge erosion and pollution from wind turbine blades," 2021.

[101] U. S. E. P. Agency. "Risk Management for Bisphenol A (BPA)." (accessed 13th July, 2023).

[102] S. Sarang. "What is BPA? Definition and Environmental Impact." OpenGrowth. (accessed 13th July, 2023).

[103] D. C. R. P. Association. "Leading Edge Erosion and Pollution from Commerical Wind Turbine Blades: Potential for BPA Released into the Environment." (accessed 29th June, 2023).

[104] B. S. Rubin, "Bisphenol A: an endocrine disruptor with widespread exposure and multiple effects," (in eng), *J Steroid Biochem Mol Biol*, vol. 127, no. 1-2, pp. 27-34, Oct 2011, doi: 10.1016/j.jsbmb.2011.05.002.

[105] O. E. Ohore and S. Zhang, "Endocrine disrupting effects of bisphenol A exposure and recent advances on its removal by water treatment systems. A review," *Scientific African*, vol. 5, p. e00135, 2019/09/01/ 2019, doi: https://doi.org/10.1016/j.sciaf.2019.e00135.

[106] Z. Wang, M. H. Alderman, C. Asgari, and H. S. Taylor, "Fetal Bisphenol-A Induced Changes in Murine Behavior and Brain Gene Expression Persisted in Adult-aged Offspring," (in eng), *Endocrinology*, vol. 161, no. 12, Dec 1 2020, doi: 10.1210/endocr/bqaa164.

[107] J. Liu, L. Zhang, G. Lu, R. Jiang, Z. Yan, and Y. Li, "Occurrence, toxicity and ecological risk of Bisphenol A analogues in aquatic environment – A review," *Ecotoxicology and Environmental Safety*, vol. 208, p. 111481, 2021/01/15/ 2021, doi: https://doi.org/10.1016/j.ecoenv.2020.111481.

[108] J. N. Pinder, "Mechanical Noise from Wind Turbines," *Wind Engineering*, vol. 16, no. 3, pp. 158-168, 1992. [Online]. Available: http://www.jstor.org/stable/43750324.

[109] W. Y. Liu, "A review on wind turbine noise mechanism and de-noising techniques," *Renewable Energy*, vol. 108, pp. 311-320, 2017/08/01/ 2017, doi: https://doi.org/10.1016/j.renene.2017.02.034.

[110] A. Patri and Y. Patnaik, "Random Forest and Stochastic Gradient Tree Boosting Based Approach for the Prediction of Airfoil Self-noise," *Procedia Computer Science*, vol. 46, 12/31 2015, doi: 10.1016/j.procs.2015.02.001.

[111] Y. Teff-Seker, O. Berger-Tal, Y. Lehnardt, and N. Teschner, "Noise pollution from wind turbines and its effects on wildlife: A cross-national analysis of current policies and planning regulations," *Renewable and Sustainable Energy Reviews*, vol. 168, p. 112801, 2022/10/01/ 2022, doi: https://doi.org/10.1016/j.rser.2022.112801.

[112] H. Wang and B. Chen, "Investigation on aerodynamic noise for leading edge erosion of wind turbine blade," *Journal of Wind Engineering and Industrial Aerodynamics*, vol. 240, p. 105484, 2023/09/01/ 2023, doi: https://doi.org/10.1016/j.jweia.2023.105484.

[113] H. Slabbekoorn, R. J. Dooling, A. N. Popper, and R. R. Fay, "Effects of anthropogenic noise on animals," 2018.

[114] A. E. Bowles, "Responses of wildlife to noise," *Wildlife and Recreationists: Coexistence through Management and Research (RL Knight and KJ Gutzwiller, Eds.). Island Press, Washington, DC,* pp. 109-156, 1995.

[115] R. Saidur, N. A. Rahim, M. R. Islam, and K. H. Solangi, "Environmental impact of wind energy," *Renewable and Sustainable Energy Reviews,* vol. 15, no. 5, pp. 2423-2430, 2011/06/01/ 2011, doi: https://doi.org/10.1016/j.rser.2011.02.024.

[116] R. J. Dooling and M. R. Leek, "Communication Masking by Man-Made Noise," in *Effects of Anthropogenic Noise on Animals*, H. Slabbekoorn, R. J. Dooling, A. N. Popper, and R. R. Fay Eds. New York, NY: Springer New York, 2018, pp. 23-46.

[117] F. Ladich, "Did Auditory Sensitivity and Vocalization Evolve Independently in Otophysan Fishes?," *Brain Behavior and Evolution,* vol. 53, no. 5-6, pp. 288-304, 1999, doi: 10.1159/000006600.

[118] A. A. Myrberg, "The effects of man-made noise on the behavior of marine animals," *Environment International*, vol. 16, no. 4, pp. 575-586, 1990/01/01/ 1990, doi: https://doi.org/10.1016/0160-4120(90)90028-5.

9.0 Appendices

Appendix 1) Leading and Trailing Edge Geometry

ANSYS Geometry	
Leading Edge	0.1m (0.1c)
Trailing Edge	0.9m (0.9c)

Appendix 2) ANSYS Meshing Parameters

Meshing Parameters	
Region 1 Sizing	
Type	Number of Divisions - 150
Behaviour	Hard
Bias	No Bias
Region 2 Sizing	
Type	Number of Divisions - 300
Behaviour	Hard
Bias	No Bias
Region 3 Sizing	
Type	Number of Divisions - 300
Behaviour	Soft
Bias	Reversed
Region 4 Sizing	
Type	Number of Divisions - 300

Behaviour	Soft
Bias	Reversed

Appendix 3) Power Coefficient and Lift to Drag Ratios

0° AoA		
Erosion Stage	**Max. Cp**	**Lift to Drag Ratio**
Clean blade	0.473	42.38
1	0.461	33.62
2	0.459	32.38
3	0.452	28.0
4	0.448	26.92
2° AoA		
Erosion Stage	**Max. Cp**	**Lift to Drag Ratio**
Clean blade	0.488	57.51
1	0.477	45.80
2	0.475	44.03
3	0.469	39.49
4	0.466	36.75
4° AoA		
Erosion Stage	**Max. Cp**	**Lift to Drag Ratio**
Clean blade	0.495	67.09
1	0.484	52.37
2	0.482	50.28

3	0.476	44.83
4	0.472	41.58
6° AoA		
Erosion Stage	**Max. Cp**	**Lift to Drag Ratio**
Clean blade	0.498	71.72
1	0.484	53.32
2	0.483	51.40
3	0.476	45.17
4	0.472	41.66
8° AoA		
Erosion Stage	**Max. Cp**	**Lift to Drag Ratio**
Clean blade	0.498	72.29
1	0.482	50.22
2	0.480	48.30
3	0.472	41.49
4	0.467	37.69
10° AoA		
Erosion Stage	**Max. Cp**	**Lift to Drag Ratio**
Clean blade	0.496	69.69
1	0.475	43.8
2	0.472	41.74
3	0.470	34.48
4	0.455	30.51

12° AoA		
Erosion Stage	**Max. Cp**	**Lift to Drag Ratio**
Clean blade	0.493	64.41
1	0.462	34.46
2	0.458	32.30
3	0.443	24.79
4	0.432	20.84
14° AoA		
Erosion Stage	**Max. Cp**	**Lift to Drag Ratio**
Clean blade	0.475	44.12
1	0.437	22.79
2	0.431	20.74
3	0.406	14.27
4	0.388	11.23

Appendix 4) ANSYS Lift and Drag Simulation Results

ANSYS Simulation Results		
Surface Roughness	0 (Clean Blade)	
AoA	**Coefficient of Lift**	**Coefficient of Drag**
0	0.4316	0.010184
2	0.64639	0.011239
4	0.85727	0.012778

6	1.0622	0.014811
8	1.259	0.017417
10	1.4449	0.020734
12	1.6134	0.02505
14	1.7533	0.03974
Surface Roughness	0.0009	
AoA (°)	**Coefficient of Lift**	**Coefficient of Drag**
0	0.4209	0.01252
2	0.6261	0.01367
4	0.8248	0.01575
6	1.012	0.01898
8	1.1831	0.02356
10	1.3258	0.03027
12	1.4177	0.04114
14	1.4175	0.06221
Surface Roughness	0.00129	
AoA (°)	**Coefficient of Lift**	**Coefficient of Drag**
0	0.4197	0.01296
2	0.62404	0.014174
4	0.01633	0.8211
6	1.00642	0.01958
8	1.1747	0.02432
10	1.3125	0.031441

12	1.3959	0.043212
14	1.3802	0.066544
Surface Roughness	0.00418	
AoA (°)	**Coefficient of Lift**	**Coefficient of Drag**
0	0.41465	0.0143
2	0.61489	0.01557
4	0.80664	0.017995
6	0.98375	0.02178
8	1.1406	0.02749
10	1.258	0.03649
12	1.309	0.052809
14	1.227	0.086
Surface Roughness	0.00760	
AoA (°)	**Coefficient of Lift**	**Coefficient of Drag**
0	0.411	0.01527
2	0.60875	0.016564
4	0.796	0.019146
6	0.96849	0.023247
8	1.1171	0.029639
10	1.2215	0.040038
12	1.2441	0.05969
14	1.1294	0.1006

Appendix 5) Lift and drag percentage change

AoA (°)	Lift decrease due to stage 1 erosion (%)	Drag Increase due to stage 1 erosion (%)
0	2.48%	22.94%
2	3.14%	21.63%
4	3.79%	23.26%
6	4.73%	28.15%
8	6.029%	35.27%
10	8.24%	45.99%
12	12.13%	64.23%
14	19.15%	56.54%
AoA (°)	**Lift decrease due to stage 2 erosion (%)**	**Drag Increase due to stage 2 erosion (%)**
0	2.76%	27.26%
2	3.46%	26.11%
4	4.22%	27.8%
6	5.25%	32.2 %
8	6.7 %	39.63%
10	9.16%	51.64%
12	13.48%	72.50%
14	21.28%	67.45%
AoA (°)	**Lift decrease due to stage 3 erosion (%)**	**Drag Increase due to stage 3 erosion (%)**

0	3.92%	40.42%
2	4.87%	38.54%
4	5.91%	40.83%
6	7.39%	47.05%
8	9.40%	57.83%
10	12.94%	75.99%
12	18.87%	110.81%
14	30.02%	116.41%
AoA (°)	**Lift decrease due to stage 4 erosion (%)**	**Drag Increase due to stage 4 erosion (%)**
0	4.77%	49.94%
2	5.82%	47.38%
4	7.15%	49.84%
6	8.82%	56.96%
8	11.27%	70.17%
10	15.46%	93.10%
12	22.89%	138.28%
14	35.58%	153.15%

Appendix 6) Onshore and Offshore Energy Losses

Year	Onshore Loss (GWh)	Offshore Loss (GWh)
1	37422.72	48712.61

2	37299.23	48551.86
3	37175.73	48391.1
4	37052.24	48230.35
5	36928.74	48069.6
6	36805.25	47908.85
7	36681.75	47748.1
8	36558.26	47587.35
9	36434.76	47426.6
10	36311.27	47265.84
11	36187.77	47105.09
12	36157.83	47066.12
13	36127.89	47027.15
14	36097.96	46988.18
15	36068.02	46949.21
16	36038.08	46910.24
17	35850.97	46666.68
18	35663.85	46423.12
19	35476.74	46179.55
20	35289.62	45935.99
21	35102.51	45692.43
22	35102.51	45692.43
23	35102.51	45692.43
24	35102.51	45692.43
25	35102.51	45692.43

Student No.